

Simulation of the diurnal variations of the oxygen isotope anomaly ($\Delta^{17}\text{O}$) of reactive atmospheric species

S. Morin¹, R. Sander², and J. Savarino³

¹Météo-France/CNRS, CNRM – GAME URA 1357, CEN, Grenoble, France

²Air Chemistry Department, Max-Planck Institute of Chemistry, P.O. Box 3060, 55020 Mainz, Germany

³CNRS/Université Joseph Fourier Grenoble 1, LGGE UMR 5183, Grenoble, France

Received: 22 November 2010 – Published in Atmos. Chem. Phys. Discuss.: 14 December 2010

Revised: 14 April 2011 – Accepted: 14 April 2011 – Published: 19 April 2011

Abstract. The isotope anomaly ($\Delta^{17}\text{O}$) of secondary atmospheric species such as nitrate (NO_3^-) or hydrogen peroxide (H_2O_2) has potential to provide useful constraints on their formation pathways. Indeed, the $\Delta^{17}\text{O}$ of their precursors (NO_x , HO_x etc.) differs and depends on their interactions with ozone, which is the main source of non-zero $\Delta^{17}\text{O}$ in the atmosphere. Interpreting variations of $\Delta^{17}\text{O}$ in secondary species requires an in-depth understanding of the $\Delta^{17}\text{O}$ of their precursors taking into account non-linear chemical regimes operating under various environmental settings.

This article reviews and illustrates a series of basic concepts relevant to the propagation of the $\Delta^{17}\text{O}$ of ozone to other reactive or secondary atmospheric species within a photochemical box model. We present results from numerical simulations carried out using the atmospheric chemistry box model CAABA/MECCA to explicitly compute the diurnal variations of the isotope anomaly of short-lived species such as NO_x and HO_x . Using a simplified but realistic tropospheric gas-phase chemistry mechanism, $\Delta^{17}\text{O}$ was propagated from ozone to other species (NO , NO_2 , OH , HO_2 , RO_2 , NO_3 , N_2O_5 , HONO , HNO_3 , HNO_4 , H_2O_2) according to the mass-balance equations, through the implementation of various sets of hypotheses pertaining to the transfer of $\Delta^{17}\text{O}$ during chemical reactions.

The model results confirm that diurnal variations in $\Delta^{17}\text{O}$ of NO_x predicted by the photochemical steady-state relationship during the day match those from the explicit treatment, but not at night. Indeed, the $\Delta^{17}\text{O}$ of NO_x is “frozen” at night

as soon as the photolytical lifetime of NO_x drops below ca. 10 min. We introduce and quantify the diurnally-integrated isotopic signature (DIIS) of sources of atmospheric nitrate and H_2O_2 , which is of particular relevance to larger-scale simulations of $\Delta^{17}\text{O}$ where high computational costs cannot be afforded.

1 Introduction

Unraveling chemical mechanisms at play in the atmosphere requires finding creative ways to test the predictions of models which describe them. Most studies to date have relied on concentration measurements to validate model results. Over the past decades alternative isotopic approaches have demonstrated great capabilities in providing concentration-independent information relevant to atmospheric processes (Laj et al., 2009; Monks et al., 2009). Of particular interest is the development of measurements of the isotope anomaly ($\Delta^{17}\text{O}$) of oxygen-bearing species (Thiemens, 2006). $\Delta^{17}\text{O}$ is defined as $\delta^{17}\text{O} - 0.52 \times \delta^{18}\text{O}$, with $\delta^x\text{O} = R^x / R_{\text{VSMOW}}^x - 1$ ($x = 17$ or 18) where R^x refers to the ${}^x\text{O}/{}^{16}\text{O}$ elemental ratio in the species of interest and in Vienna Standard Mean Ocean Water (VSMOW), taken as a reference. Ozone (O_3) possesses a distinctive isotope anomaly inherited from non-mass dependent fractionation NMDF during its formation in the atmosphere (Marcus, 2008).

In contrast to conventional isotopic ratios which are strongly affected by isotopic fractionation, $\Delta^{17}\text{O}$ is fairly insensitive to mass-dependent fractionation. The vast majority of chemical reactions induce mass-dependent fractionation, which in general do not strongly modify $\Delta^{17}\text{O}$. It can thus be reasonably assumed that $\Delta^{17}\text{O}$ is transferred as is during



Correspondence to: S. Morin
(samuel.morin@meteo.fr)

oxidation reactions in the atmosphere, although this consideration is sometimes challenged when dealing with species possessing small $\Delta^{17}\text{O}$ values (Kaiser et al., 2004). As a result, $\Delta^{17}\text{O}$ of a given species generally simply reflects the fractional importance in its elemental composition of oxygen atoms inherited directly or indirectly from ozone. This behavior has opened large possibilities to explore atmospheric oxidation mechanisms using $\Delta^{17}\text{O}$ signatures (Lyons, 2001; Michalski et al., 2003; Thiemens, 2006; Savarino et al., 2000; Savarino and Morin, 2011).

One area of intense research on the interpretation of $\Delta^{17}\text{O}$ signatures is the case of inorganic atmospheric nitrate ($\text{HNO}_3 + \text{particulate } \text{NO}_3^-$), referred to as atmospheric nitrate (NO_3^-) below. Indeed, atmospheric nitrate is the final oxidation product of nitrogen oxides ($\text{NO}_x = \text{NO} + \text{NO}_2$), which are of primary importance for air-quality (Jacob, 1999; Finlayson-Pitts and Pitts, 2000; Brown et al., 2006). The development of sensitive methods to analyze the oxygen isotopic composition of nitrate (Michalski et al., 2002; Kaiser et al., 2007) makes it possible to obtain $\Delta^{17}\text{O}$ of atmospheric nitrate at weekly to sub-daily timescales in most environments. This has been used in the recent past to study the seasonal variations in NO_x oxidation pathways in mid-latitudes (Michalski et al., 2003; Tsunogai et al., 2010) and polar (Morin et al., 2008, 2009; Kunasek et al., 2008) regions, the nature of the sources of atmospheric nitrate in the Antarctic lower atmosphere (Savarino et al., 2007; McCabe et al., 2007; Frey et al., 2009), and more recently the global-scale variations in NO_x sink reactions (Alexander et al., 2009). $\Delta^{17}\text{O}$ of nitrate has also been used to identify long-term changes in the oxidative properties of the Earth atmosphere, from centennial (Alexander et al., 2004) to millennial (Erblund et al., 2009) time scales.

While including the isotopic composition of long-lived tracers (e.g. CO_2 , N_2O etc.) into global biogeochemical models of the carbon and nitrogen cycle has proved extremely successful (e.g., Hoag et al., 2005), embedding the $\Delta^{17}\text{O}$ of short-lived reactive compounds into atmospheric photochemical models has only recently gained increased attention (Lyons, 2001; Michalski et al., 2003; Zahn et al., 2006; Dominguez et al., 2009; Gromov et al., 2010; Michalski and Xu, 2010). Current hope within the “atmospheric geochemistry community” is that $\Delta^{17}\text{O}$ data can help solve atmospheric chemistry issues such as ascertaining the relative role of heterogeneous reactions in NO_x sink mechanisms (i.e. what is the exact role of N_2O_5 hydrolysis; Brown et al., 2006). However, inferring quantitative atmospheric information from $\Delta^{17}\text{O}$ of nitrate requires assessing precisely its controls and to include them into a consistent modeling framework. In the last few years, several models have been proposed to study the spatio-temporal variations of $\Delta^{17}\text{O}$ and relate them to spatio-temporal variations of the fractional contribution of NO_x sink reactions. The pioneering work of Lyons (2001) set the stage for the first model study of the seasonal variations of $\Delta^{17}\text{O}$ of atmospheric nitrate by Michalski et al. (2003). Further implementations of $\Delta^{17}\text{O}$

into atmospheric chemistry models were proposed in the following years, from 0-D box-modeling (Morin et al., 2008; Dominguez et al., 2009; Michalski and Xu, 2010) to the 3-D chemical transport model GEOS-Chem (Kunasek et al., 2008; Alexander et al., 2009).

This study revisits some assumptions, hypotheses and approaches previously introduced in the literature (e.g. Michalski et al., 2003; Morin et al., 2007, 2008, 2009; Kunasek et al., 2008; Alexander et al., 2009) and puts them within a consistent framework and perspective that makes it easier to understand and implement in existing atmospheric chemistry models. Limitations of the various assumptions that have been used so far are highlighted and critically evaluated. The overarching goal is to provide a rationale behind assumptions and simplifications that have to be used in large scale model implementation in order to reduce computing costs. The CAABA/MECCA atmospheric chemistry box model (Sander et al., 2011) was used to explicitly calculate the time evolution of the $\Delta^{17}\text{O}$ of short-lived reactive species at each time step. Model runs were performed in a few simple cases to demonstrate the usefulness of such assessments and provide the basis of future analogous studies. Finally, recommendations are given for the implementation of simplifying assumptions into large-scale atmospheric chemistry models.

2 General framework

2.1 The general “mass-balance” equation

The general “mass-balance” equation (also termed the “continuity equation”) governing the temporal evolution of the concentration of a given species in a given air parcel is given by:

$$\frac{d}{dt}[\text{X}] = \sum_i P_i - \sum_j L_j \quad (1)$$

where P_i and L_j represent source and sink rates (in $\text{cm}^{-3} \text{s}^{-1}$) of the species X, respectively. Its atmospheric concentration, denoted $[\text{X}]$, is expressed in cm^{-3} . Sources and sinks include both chemical reactions within the parcel and fluxes at its boundaries. Atmospheric chemistry models are mostly driven by reaction kinetics, so that the chemical components of P_i and L_j are simply expressed as a reaction rate constant (usually referred to as k values) times the relevant atmospheric concentrations (Jacob, 1999; Finlayson-Pitts and Pitts, 2000).

The implementation of $\Delta^{17}\text{O}$ into the mass balance Eq. (1) follows from mass conservation applied to the oxygen isotope anomaly. Of course, this rather simple method would not apply to isotopic enrichment (δ) values, because isotopic fractionation has to be fully taken into account for every reaction considered (Gromov et al., 2010). The key assumption behind the modeling approach is that sink reactions do not

induce a specific non-mass dependent fractionation, and that every source reaction induces the transfer of a given $\Delta^{17}\text{O}$ value to the newly produced species. Potential contributions of mass-dependent fractionation to the time evolution of $\Delta^{17}\text{O}$ are neglected, because we concentrate on species generally possessing high $\Delta^{17}\text{O}$ values where such effects are negligible (Kaiser et al., 2004). The $\Delta^{17}\text{O}$ mass-balance equation reads:

$$\frac{d}{dt} ([\text{X}] \times \Delta^{17}\text{O}(\text{X})) = \sum_i (P_i \times \Delta^{17}\text{O}_i(\text{X})) - (\sum_j L_j) \times \Delta^{17}\text{O}(\text{X}) \quad (2)$$

where $\Delta^{17}\text{O}(\text{X})$ represents the $\Delta^{17}\text{O}$ of the species X and $\Delta^{17}\text{O}_i(\text{X})$ is the isotope anomaly that is transferred to X through the production channel P_i of the species X. It is estimated as a function of the $\Delta^{17}\text{O}$ value of the precursors involved in a given production channel for species X, using a mass-balance approach based on the counting of the oxygen atoms transferred throughout a given production channel. Non-mass dependent fractionation induced by a specific reaction can also be taken into account in the equation above. Solving numerically the system of equations formed by Eqs. (1) and (2) for all relevant atmospheric species simultaneously yields the time evolution of the concentration and $\Delta^{17}\text{O}$ of each atmospheric species. This is generally not computationally affordable for large-scale modeling studies such as Alexander et al. (2009). The computation can be carried out for limited periods of time using box models.

2.2 Isotopic exchange reactions

Not only chemical production and destruction impact the $\Delta^{17}\text{O}$ of a given species. Isotopic exchange reactions can also modify it. Their main characteristic is that they have no impact on the chemical budget of a species (i.e., Eq. (1) is not changed), but they have an impact on the isotopic mass-balance Eq. (2). The magnitude of an isotopic exchange reaction can be expressed in a similar manner to chemical production or destruction fluxes. In what follows, the rate of the k isotopic exchange reaction is referred to as E_k ; the ultimate $\Delta^{17}\text{O}$ value that would be attained in species X if the isotopic exchange with the species Y_k fully proceeds is noted $\Delta^{17}\text{O}(Y_k)$. Implementing this into Eq. (2) yields:

$$\begin{aligned} \frac{d}{dt} ([\text{X}] \times \Delta^{17}\text{O}(\text{X})) &= \sum_i (P_i \times \Delta^{17}\text{O}_i(\text{X})) \\ &+ \sum_k (E_k \times \Delta^{17}\text{O}(Y_k)) - (\sum_j L_j + \sum_k E_k) \times \Delta^{17}\text{O}(\text{X}) \end{aligned} \quad (3)$$

2.3 Steady-state approximation

A very commonly used simplification in atmospheric chemistry models is the so-called “photochemical steady-state (PSS)” approximation. This simply assumes that the photolytical lifetime of a given species is sufficiently short that the short-term variations of its concentration are negligible, i.e. $\frac{d}{dt}[\text{X}] \approx 0$. In other words, a near-perfect balance between

sources and sinks for a given species is assumed. Implementing this assumption into the isotopic mass-balance Eq. (2), and taking into account that, at PSS, $\sum_i P_i = \sum_j L_j$ yields:

$$\Delta^{17}\text{O}(\text{X}) = \frac{\sum_i (P_i \times \Delta^{17}\text{O}_i(\text{X}))}{\sum_i P_i} \quad (4)$$

Stated differently, at PSS the $\Delta^{17}\text{O}$ of a given species is instantaneously equal to the $\Delta^{17}\text{O}$ induced by the combination of its different chemical sources, scaled according to their relative strength, as shown in Eq. (4). Without PSS, the time evolution of the $\Delta^{17}\text{O}$ of a given species must also take into account its $\Delta^{17}\text{O}$ value earlier on. The longer the lifetime of a given species, the slower the time evolution of its $\Delta^{17}\text{O}$.

2.4 Controls on $\Delta^{17}\text{O}$ of atmospheric nitrate and hydrogen peroxide H_2O_2

2.4.1 Atmospheric nitrate

Atmospheric nitrate is formed homogeneously and heterogeneously in the atmosphere through the following reactions (Jacob, 1999; Finlayson-Pitts and Pitts, 2000):



Here, RH represents a generic hydrocarbon. Dry and wet deposition are the main sinks of atmospheric nitrate, controlling its atmospheric lifetime which is on the order of days to weeks (Finlayson-Pitts and Pitts, 2000). A straightforward rearrangement of Eq. (2) yields the equation governing the time evolution of $\Delta^{17}\text{O}$ of atmospheric nitrate:

$$\frac{d}{dt} ([\text{NO}_3^-] \times \Delta^{17}\text{O}(\text{NO}_3^-)) = \sum_i (P_i \times \Delta^{17}\text{O}_i(\text{NO}_3^-)) - \frac{[\text{NO}_3^-]}{\tau} \times \Delta^{17}\text{O}(\text{NO}_3^-) \quad (5)$$

where τ is the atmospheric lifetime of atmospheric nitrate. $\Delta^{17}\text{O}_i(\text{NO}_3^-)$ values can be calculated for each nitrate production channel (Michalski et al., 2003; Morin et al., 2007, 2009; Kunasek et al., 2008):

$$\Delta^{17}\text{O}_{\text{OH}+\text{NO}_2}(\text{NO}_3^-) = 1/3 \times \Delta^{17}\text{O}(\text{OH}) + 2/3 \times \Delta^{17}\text{O}(\text{NO}_2) \quad (6)$$

$$\Delta^{17}\text{O}_{\text{NO}_3+\text{RH}}(\text{NO}_3^-) = \Delta^{17}\text{O}(\text{NO}_3) \quad (7)$$

$$\Delta^{17}\text{O}_{\text{N}_2\text{O}_5\text{hydrol}}(\text{NO}_3^-) = 5/6 \times \Delta^{17}\text{O}(\text{N}_2\text{O}_5) \quad (8)$$

$$\Delta^{17}\text{O}_{\text{HNO}_4\text{hydrol}}(\text{NO}_3^-) = \Delta^{17}\text{O}(\text{HNO}_4) \quad (9)$$

As will be demonstrated below, both the mixing ratio and the $\Delta^{17}\text{O}$ of nitrate precursors vary diurnally. For instance, OH plays a significant role only during the day, and $\Delta^{17}\text{O}(\text{NO}_2)$ exhibits a strong diurnal variation with a minimum during the day and a maximum at night. Clearly, only the daytime $\Delta^{17}\text{O}(\text{NO}_2)$ values matter for the $\text{OH} + \text{NO}_2$ nitrate production channel, since during the night this reaction is suppressed. To account for the fact that the isotopic signature of a given production channel has to be scaled with its strength, we define the diurnally-integrated isotopic signature (DIIS) of the nitrate source, denoted $\overline{\Delta^{17}\text{O}_i(\text{NO}_3^-)}$, as follows:

$$\overline{\Delta^{17}\text{O}_i(\text{NO}_3^-)} = \frac{\int_0^{24\text{h}} P_i \times \Delta^{17}\text{O}_i(\text{NO}_3^-) dt}{\int_0^{24\text{h}} P_i dt} \quad (10)$$

DIIS values quantify the overall $\Delta^{17}\text{O}$ inherited from a given source reaction, taking into account the scaling of diurnal variations in its strength with the associated $\Delta^{17}\text{O}$ it transfers. Additionally, DIIS is a useful metric to quantify the impact of various environmental settings or hypotheses pertaining to isotopic transfer on the ultimate $\Delta^{17}\text{O}$ of atmospheric nitrate.

In the case where the atmospheric lifetime of a given secondary species is significantly longer than one day, DIIS values can be used to infer the seasonal variations of $\Delta^{17}\text{O}$ from the following equation, virtually assuming that steady-state applies:

$$\Delta^{17}\text{O}(\text{NO}_3^-) = \frac{\sum_i (P_i \times \overline{\Delta^{17}\text{O}_i(\text{NO}_3^-)})}{\sum_i P_i} \quad (11)$$

Equation (11) takes into account that both P_i and $\overline{\Delta^{17}\text{O}_i(\text{NO}_3^-)}$ values change seasonally or as a function of environmental conditions. This method was implicitly used originally by Michalski et al. (2003) to study the seasonal variations of $\Delta^{17}\text{O}(\text{NO}_3^-)$ in coastal California. While correct at the seasonal scale to study seasonal variation of nitrate as far as its lifetime is significantly larger than several days, this method does not adequately address variations of $\Delta^{17}\text{O}(\text{NO}_3^-)$ at temporal scale smaller than its atmospheric lifetime (Michalski and Xu, 2010), because sink reactions (both physical and chemical) must then be explicitly taken into account, as shown by Eq. (5).

2.4.2 Hydrogen peroxide (H_2O_2)

Hydrogen peroxide is a key atmospheric oxidant which plays a major role for in-cloud oxidation of S(IV) (Finlayson-Pitts and Pitts, 2000; Alexander et al., 2005). Savarino and Thiemens (1999a) demonstrated that it possesses a small but significant $\Delta^{17}\text{O}$ signature, which has then been used to study the partitioning between various S(IV) oxidants in the

atmosphere (Savarino et al., 2000; Alexander et al., 2005). H_2O_2 is mostly formed through the self reaction of HO_2 :



The $\Delta^{17}\text{O}$ inherited by H_2O_2 during the above reaction is equal to $\Delta^{17}\text{O}(\text{HO}_2)$. Indeed, Zhu and Lin (2001) have shown that the most likely mechanism for the self reaction of HO_2 involves a six-member-ring intermediate through head-to-tail association, which implies that the two oxygen atoms in H_2O_2 originate from a single one HO_2 radical out of the two reactants.

The concept of DIIS applies to H_2O_2 in a manner analogous to atmospheric nitrate (see above). Since Reaction (R5) is the sole significant H_2O_2 production pathway, and because the atmospheric lifetime of H_2O_2 is generally larger than one day, the application of Eq. (11) is trivial and shows that seasonal variations of $\Delta^{17}\text{O}(\text{H}_2\text{O}_2)$ can directly be inferred from variations of $\overline{\Delta^{17}\text{O}_{\text{HO}_2+\text{HO}_2}(\text{H}_2\text{O}_2)}$ at first order.

3 Material and methods: numerical experiments on $\Delta^{17}\text{O}$ of short-lived species

In this study, we focus on the time evolution of the $\Delta^{17}\text{O}$ of short-lived atmospheric reactive species such as HO_x ($= \text{OH} + \text{HO}_2$), NO_x ($= \text{NO} + \text{NO}_2$) and RO_2 . For simplicity, in this initial study we restrict our analysis to gas-phase reactions and exclude halogen, sulfur and carbonaceous chemistry, to focus on the highly non-linear $\text{NO}_x\text{-HO}_x/\text{RO}_x\text{-O}_3$ chemistry first. The impact of diurnal variations of $\Delta^{17}\text{O}$ of short-lived species on secondary species such as atmospheric nitrate and H_2O_2 is explored through the estimation of diurnally-integrated isotopic signature (DIIS) of these species. This series of 51 reactions (including 14 photolysis reactions) represents a subset of the chemical mechanism implemented in MECCA (Sander et al., 2011) suited for simplified analysis in the remote marine boundary layer. The complete listing of the reactions considered is given as an online supplement to this article. Note that this article mostly seeks to illustrate the basic concepts and equations introduced in Sect. 2, and the impact of performing various hypotheses to propagate the $\Delta^{17}\text{O}$ of ozone throughout atmospheric reactions. This is why heterogeneous reactions leading to the formation of atmospheric nitrate are not explicitly included in the model, because doing so would render the illustration of the main concepts unnecessarily tedious. We concentrate on gas-phase reactions, which provide illustrations of the main behaviors described here, and leave the explicit inclusion of heterogeneous chemistry in the model for a follow-up study comparing observed and simulated diurnal variations of $\Delta^{17}\text{O}(\text{NO}_3^-)$.

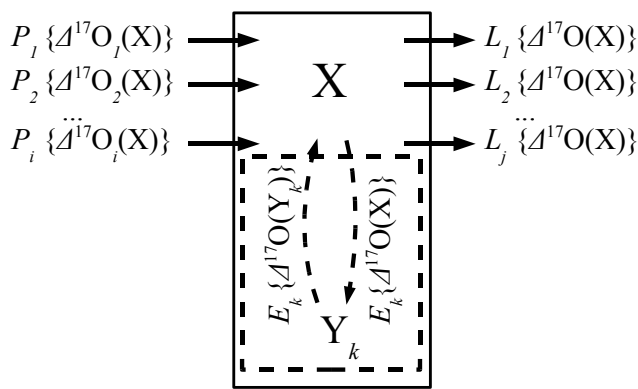


Fig. 1. Schematic representing the isotopic mass-balance equation including one isotopic exchange reaction. Arrows represent production (or destruction) fluxes. The flux is given by the P , L and E terms, while the corresponding transferred $\Delta^{17}\text{O}$ value is given in brackets. The solid box represent the chemical budget of the species X , while the dashed box takes into account the full isotopic budget of the species X . The scheme illustrates that isotopic exchange reactions have no impact on the chemical budget of a given species X .

3.1 Species with assigned $\Delta^{17}\text{O}$ values

3.1.1 $\Delta^{17}\text{O}(\text{H}_2\text{O})$ and $\Delta^{17}\text{O}(\text{O}_2)$

Because they represent large oxygen reservoirs with a negligible isotope anomaly, we assume in what follows that $\Delta^{17}\text{O}$ of water vapor (H_2O) and molecular oxygen (O_2) are constant, with a value of insignificantly different from 0‰ (Barkan and Luz, 2003, 2005), in comparison to the $\Delta^{17}\text{O}$ of the species dealt with below. Indeed, $\Delta^{17}\text{O}(\text{O}_2) = -0.3\text{‰}$ (Barkan and Luz, 2003), while $\Delta^{17}\text{O}(\text{H}_2\text{O})$ ranges between -1.0 and 0.0‰ (Barkan and Luz, 2005). This simplification is generally made in modeling studies dealing with $\Delta^{17}\text{O}(\text{NO}_3^-)$ (Michalski et al., 2003; Alexander et al., 2009), and allows to focus on and interpret the changes in $\Delta^{17}\text{O}$ of reactive and secondary species attributable to chemical transfer of $\Delta^{17}\text{O}$ from ozone.

3.1.2 $\Delta^{17}\text{O}(\text{O}_3)$

Although several atmospheric reactions induce non-mass dependent fractionation (Brenninkmeijer et al., 2003; Thiemens, 2006) and thus may contribute significantly to the non-zero $\Delta^{17}\text{O}$ values of several atmospheric species, the overwhelming source of non-zero $\Delta^{17}\text{O}$ in the lower atmosphere is ozone (O_3). As repeatedly mentioned in the recent literature (e.g. Morin et al., 2007; Michalski and Bhattacharya, 2009; Alexander et al., 2009; Dominguez et al., 2009), the tropospheric value of $\Delta^{17}\text{O}(\text{O}_3)$ is controversial. In addition, ozone is isotopically asymmetrical (Janssen, 2005; Marcus, 2008), meaning that the $\Delta^{17}\text{O}$ borne by its terminal and central atoms are different. Furthermore, oxy-

gen atoms of O_3 are not chemically equivalent in terms of reactivity during bimolecular reactions. We define $\Delta^{17}\text{O}(\text{O}_3^*)$ as the $\Delta^{17}\text{O}$ value which is transferred along with the terminal O atom of ozone. The motivation for this choice is two-fold. Firstly, terminal oxygen atoms generally have a greater probability of being transferred than the central oxygen atom (Savarino et al., 2008), and this probability even equals 1 for the following reactions: $\text{O}_3 + \text{Ag}_{\text{metal}}$ (Bhattacharya et al., 2008), $\text{O}_3 + \text{NO}_2^-$ (Liu et al., 2001; Michalski and Bhattacharya, 2009), $\text{O}_3 + \text{NO}_2$ (Peiro-Garcia and Nebot-Gil, 2003, Berhanu and Bhattacharya, personal communication, 2011). Secondly, we note that atmospheric direct measurements of $\Delta^{17}\text{O}(\text{O}_3^*)$ are now possible using the reaction $\text{O}_3 + \text{NO}_2^-$ as a chemical probe (Michalski and Bhattacharya, 2009; Vicars et al., 2011). $\Delta^{17}\text{O}(\text{O}_3^*)$, which may be referred to as the “transferrable $\Delta^{17}\text{O}(\text{O}_3)$ values through bimolecular reactions operating through the terminal O atom of ozone”, can now be directly measured.

The link between $\Delta^{17}\text{O}(\text{O}_3)$ and $\Delta^{17}\text{O}(\text{O}_3^*)$ is complex due to our currently limited knowledge of the intramolecular distribution of $\Delta^{17}\text{O}$ within the ozone molecule. For $\Delta^{17}\text{O}(\text{O}_3)$ values ranging between 20 and 40‰, currently existing experimental data yield the following relationship:

$$\Delta^{17}\text{O}(\text{O}_3^*) = 1.5 \times \Delta^{17}\text{O}(\text{O}_3) \quad (12)$$

We note that, although this is not entirely consistent with the full range of experimental observations and their theoretical implications, this equation is equivalent to considering that $\Delta^{17}\text{O}$ resides exclusively on the terminal oxygen atoms of ozone (Michalski and Bhattacharya, 2009).

Consistent with the modeling studies carried out hitherto (Michalski et al., 2003; Morin et al., 2008; Kunasek et al., 2008; Alexander et al., 2009; Dominguez et al., 2009; Michalski and Xu, 2010), we use a constant value of $\Delta^{17}\text{O}(\text{O}_3)$ of 30‰, which falls within the 25–35‰ range generally found in the literature (see Brenninkmeijer et al. (2003) or Morin et al. (2007) for details), to illustrate the results of the calculations. Most results of the present work can be extrapolated to different $\Delta^{17}\text{O}(\text{O}_3)$ values simply by scaling them with the ratio of a different value of $\Delta^{17}\text{O}(\text{O}_3)$ to our current choice. Note that while we have chosen a constant value for $\Delta^{17}\text{O}(\text{O}_3)$ to remain consistent with previous studies, the model can account for temporal variations of $\Delta^{17}\text{O}(\text{O}_3)$ (Vicars et al., 2011). Should $\Delta^{17}\text{O}(\text{O}_3)$ exhibit significant diurnal variations, the quantitative results provided below for illustration purposes would need to be revised, but the underlying concepts exposed here would remain valid. In this case, only an explicit modeling framework as described here would then be suitable to compute the $\Delta^{17}\text{O}$ values of reactive and secondary atmospheric species.

In this work, bimolecular reactions involving ozone are:



Table 1. Listing of $\Delta^{17}\text{O}_i(\text{X})$ relevant to Case 1 (PSS NO_x), if not given in Sect. 3.2.1. Note the special case of HNO_4 and N_2O_5 , for which the $\Delta^{17}\text{O}$ of each of the molecule making up the dimer are explicitly referred to and tracked.

Rxn #	$\Delta^{17}\text{O}_i(\text{X})$
G3109 $\text{NO}_3 + \text{NO}_2 \rightarrow \text{N}_2\text{O}_5$	$\Delta^{17}\text{O}_{\text{G}3109}(\text{N}_2\text{O}_5 - \text{NO}_2) = \Delta^{17}\text{O}(\text{NO}_2)$ $\Delta^{17}\text{O}_{\text{G}3109}(\text{N}_2\text{O}_5 - \text{NO}_3) = \Delta^{17}\text{O}(\text{NO}_3)$
G3200 $\text{NO} + \text{OH} \rightarrow \text{HONO}$	$\Delta^{17}\text{O}_{\text{G}3200}(\text{HONO}) = 1/2 (\Delta^{17}\text{O}(\text{NO}) + \Delta^{17}\text{O}(\text{OH}))$
G3202 $\text{NO}_2 + \text{OH} \rightarrow \text{HNO}_3$	$\Delta^{17}\text{O}_{\text{G}3202}(\text{HNO}_3) = 1/3 (2\Delta^{17}\text{O}(\text{NO}_2) + \Delta^{17}\text{O}(\text{OH}))$
G3203 $\text{NO}_2 + \text{HO}_2 (+\text{M}) \rightarrow \text{HNO}_4$	$\Delta^{17}\text{O}_{\text{G}3203}(\text{HNO}_4 - \text{NO}_2) = \Delta^{17}\text{O}(\text{NO}_2)$
G4109 $\text{HCHO} + \text{NO}_3 (+\text{O}_2) \rightarrow \text{HNO}_3 + \text{CO} + \text{HO}_2$	$\Delta^{17}\text{O}_{\text{G}4109}(\text{HNO}_3) = \Delta^{17}\text{O}(\text{NO}_3)$



Ab initio calculations on the mechanism of the reaction $\text{NO}_2 + \text{O}_3$ reveal that it proceeds through the abstraction of the terminal O atom of ozone (Peiro-Garcia and Nebot-Gil, 2003). In addition, the transfer of $\Delta^{17}\text{O}$ through reaction $\text{NO}_2 + \text{O}_3$ has been recently studied in the lab and it was also concluded that only the terminal O atom of ozone is transferred (Berhanu and Bhattacharya, personal communication, 2011). We also assume that the $\text{OH} + \text{O}_3$ reaction proceeds exclusively through the transfer of the terminal O atom of ozone. We thus apply $\Delta^{17}\text{O}(\text{O}_3^\star)$ as the isotopic signature of these reactions. Considering a $\Delta^{17}\text{O}(\text{O}_3)$ value of 30‰, this corresponds to $\Delta^{17}\text{O}(\text{O}_3^\star) = 45\text{‰}$. In the case of the reaction $\text{NO} + \text{O}_3$, we apply the $\Delta^{17}\text{O}$ transfer rate determined experimentally by Savarino et al. (2008):

$$\Delta^{17}\text{O}_{\text{NO}+\text{O}_3}(\text{NO}_2) = 1.18 \times \Delta^{17}\text{O}(\text{O}_3) + 6.6 \times 10^{-3} \quad (13)$$

With a $\Delta^{17}\text{O}(\text{O}_3)$ value of 30‰, this corresponds to a $\Delta^{17}\text{O}_{\text{NO}+\text{O}_3}(\text{NO}_2)$ value of 42‰. The fact that the $\Delta^{17}\text{O}(\text{O}_3)$ transferred through this reaction is lower than through reactions described before stems from the fact that not only the terminal, but also the central oxygen atom of ozone reacts with NO, as described in detail by Savarino et al. (2008). Lastly, in the case of reaction $\text{HO}_2 + \text{O}_3$ this is irrelevant to the value of $\Delta^{17}\text{O}(\text{OH})$ because the oxygen atom in OH stems from HO_2 , not ozone.

3.1.3 $\Delta^{17}\text{O}(\text{RO}_2)$

In this study we explicitly separate HO_2 from other peroxy radicals, denoted RO_2 where R represents a carbonaceous chain, because the chemical budget of HO_2 and RO_2 is very different. While reactions involving ozone contribute to the budget of HO_2 , the only source of RO_2 is the reaction between O_2 and a R radical. Since $\Delta^{17}\text{O}(\text{O}_2) = 0\text{‰}$ (see above), this immediately implies that $\Delta^{17}\text{O}(\text{RO}_2) = 0\text{‰}$ under all tropospheric conditions.

3.2 Overview of the sets of hypotheses regarding the $\Delta^{17}\text{O}$ transfer throughout chemical reactions

Below we present the various sets of hypotheses (numbered Cases 1 to 6) implemented to compute the time evolution of $\Delta^{17}\text{O}$ of the species of interest using various assumptions in terms of $\Delta^{17}\text{O}$ transfer.

3.2.1 Case 1: NO_x photochemical steady-state (PSS) and basic hypotheses

- OH, HO_2 : $\Delta^{17}\text{O}$ of both species is equal to 0‰.
- $\text{NO}, \text{NO}_2, \text{NO}_3$: The $\Delta^{17}\text{O}$ of these species is calculated using PSS:

$$\Delta^{17}\text{O}(\text{NO}_2) = \alpha \times \Delta^{17}\text{O}_{\text{NO}+\text{O}_3}(\text{NO}_2)$$

with

$$\alpha = \frac{k_{\text{NO}+\text{O}_3}[\text{O}_3]}{k_{\text{NO}+\text{O}_3}[\text{O}_3] + k_{\text{NO}+\text{HO}_2}[\text{HO}_2] + k_{\text{NO}+\text{RO}_2}[\text{RO}_2]}$$

as defined by Michalski et al. (2003) and demonstrated in Morin et al. (2007). It follows from PSS that $\Delta^{17}\text{O}(\text{NO}) = \Delta^{17}\text{O}(\text{NO}_2)$. $\Delta^{17}\text{O}(\text{NO}_3)$ is given as:

$$\Delta^{17}\text{O}(\text{NO}_3) = 1/3 (2\alpha \Delta^{17}\text{O}_{\text{NO}+\text{O}_3}(\text{NO}_2) + \Delta^{17}\text{O}(\text{O}_3^\star))$$

- $\text{HONO}, \text{HNO}_3, \text{H}_2\text{O}_2$: the calculation of $\Delta^{17}\text{O}$ is calculated following Eq. (2).
- $\text{N}_2\text{O}_5, \text{HNO}_4$: both these species are dimers formed by the combinations of two radicals (NO_2 and NO_3 , and NO_2 and HO_2 , respectively). This makes necessary to track the time evolution of the $\Delta^{17}\text{O}$ of both components of the dimer making up N_2O_5 and HNO_4 , respectively, since their O atoms are not isotopically equivalents.

Table 1 gives the $\Delta^{17}\text{O}_i(\text{X})$ values for each species produced, if different from 0 and not given above.

Table 2. $\Delta^{17}\text{O}_i(\text{X})$ for Case 2 (explicit NO_x). Only equations featuring different $\Delta^{17}\text{O}_i(\text{X})$ than in Case 1 (PSS NO_x) are presented here.

Rxn #	$\Delta^{17}\text{O}_i(\text{X})$
G3103 $\text{NO} + \text{O}_3 \rightarrow \text{NO}_2 + \text{O}_2$	$\Delta^{17}\text{O}_{\text{G3103}}(\text{NO}_2) = 1/2 (\Delta^{17}\text{O}_{\text{NO}+\text{O}_3}(\text{NO}_2) + \Delta^{17}\text{O}(\text{NO}))$
G3106 $\text{NO}_2 + \text{O}_3 \rightarrow \text{NO}_3 + \text{O}_2$	$\Delta^{17}\text{O}_{\text{G3106}}(\text{NO}_3) = 1/2 (\Delta^{17}\text{O}(\text{O}_3^\star) + \Delta^{17}\text{O}(\text{NO}_2))$
G3108 $\text{NO}_3 + \text{NO} \rightarrow 2\text{NO}_2$	$\Delta^{17}\text{O}_{\text{G3108}}(\text{NO}_2) = 1/2 (\Delta^{17}\text{O}(\text{NO}_3) + \Delta^{17}\text{O}(\text{NO}))$
G3110 $\text{N}_2\text{O}_5(+\text{M}) \rightarrow \text{NO}_2 + \text{NO}_3$	$\Delta^{17}\text{O}_{\text{G3110}}(\text{NO}_2) = 1/2 (\Delta^{17}\text{O}(\text{N}_2\text{O}_5 - \text{NO}_2) + \Delta^{17}\text{O}(\text{N}_2\text{O}_5 - \text{NO}_3))$ $\Delta^{17}\text{O}_{\text{G3110}}(\text{NO}_3) = 1/3 (\Delta^{17}\text{O}(\text{N}_2\text{O}_5 - \text{NO}_2) + 2\Delta^{17}\text{O}(\text{N}_2\text{O}_5 - \text{NO}_3))$
G3201 $\text{NO} + \text{HO}_2 \rightarrow \text{NO}_2 + \text{OH}$	$\Delta^{17}\text{O}_{\text{G3201}}(\text{NO}_2) = 1/2 (\Delta^{17}\text{O}(\text{HO}_2) + \Delta^{17}\text{O}(\text{NO}))$
G3204 $\text{NO}_3 + \text{HO}_2 \rightarrow \text{NO}_2 + \text{OH} + \text{O}_2$	$\Delta^{17}\text{O}_{\text{G3204}}(\text{NO}_2) = \Delta^{17}\text{O}(\text{NO}_3)$
G3205 $\text{HONO} + \text{OH} \rightarrow \text{NO}_2 + \text{H}_2\text{O}$	$\Delta^{17}\text{O}_{\text{G3205}}(\text{NO}_2) = \Delta^{17}\text{O}(\text{HONO})$
G3206 $\text{HNO}_3 + \text{OH} \rightarrow \text{H}_2\text{O} + \text{NO}_3$	$\Delta^{17}\text{O}_{\text{G3206}}(\text{NO}_3) = \Delta^{17}\text{O}(\text{HNO}_3)$
G3207 $\text{HNO}_4(+\text{M}) \rightarrow \text{NO}_2 + \text{HO}_2$	$\Delta^{17}\text{O}_{\text{G3207}}(\text{NO}_2) = \Delta^{17}\text{O}(\text{HNO}_4 - \text{NO}_2)$
G3208 $\text{HNO}_4 + \text{OH} \rightarrow \text{NO}_2 + \text{H}_2\text{O} + \text{O}_2$	$\Delta^{17}\text{O}_{\text{G3208}}(\text{NO}_2) = \Delta^{17}\text{O}(\text{HNO}_4 - \text{NO}_2)$
G4104 $\text{CH}_3\text{O}_2 + \text{NO} \rightarrow \text{HCHO} + \text{NO}_2 + \text{HO}_2$	$\Delta^{17}\text{O}_{\text{G4104}}(\text{NO}_2) = 1/2 \Delta^{17}\text{O}(\text{NO})$
G4105 $\text{CH}_3\text{O}_2 + \text{NO}_3 \rightarrow \text{HCHO} + \text{HO}_2 + \text{NO}_2$	$\Delta^{17}\text{O}_{\text{G4105}}(\text{NO}_2) = \Delta^{17}\text{O}(\text{NO}_3)$
J3101 $\text{NO}_2 + \text{h}\nu \rightarrow \text{NO} + \text{O}({}^3\text{P})$	$\Delta^{17}\text{O}_{\text{J3101}}(\text{NO}) = \Delta^{17}\text{O}(\text{NO}_2)$
J3103a $\text{NO}_3 + \text{h}\nu \rightarrow \text{NO}_2 + \text{O}({}^3\text{P})$	$\Delta^{17}\text{O}_{\text{J3103a}}(\text{NO}_2) = \Delta^{17}\text{O}(\text{NO}_3)$
J3103b $\text{NO}_3 + \text{h}\nu \rightarrow \text{NO} + \text{O}_2$	$\Delta^{17}\text{O}_{\text{J3103b}}(\text{NO}) = \Delta^{17}\text{O}(\text{NO}_3)$
J3104a $\text{N}_2\text{O}_5 + \text{h}\nu \rightarrow \text{NO}_2 + \text{NO}_3$	$\Delta^{17}\text{O}_{\text{J3104a}}(\text{NO}_2) = 1/2 (\Delta^{17}\text{O}(\text{N}_2\text{O}_5 - \text{NO}_2) + \Delta^{17}\text{O}(\text{N}_2\text{O}_5 - \text{NO}_3))$ $\Delta^{17}\text{O}_{\text{J3104a}}(\text{NO}_3) = 1/3 (\Delta^{17}\text{O}(\text{N}_2\text{O}_5 - \text{NO}_2) + 2\Delta^{17}\text{O}(\text{N}_2\text{O}_5 - \text{NO}_3))$
J3200 $\text{HONO} + \text{h}\nu \rightarrow \text{OH} + \text{NO}$	$\Delta^{17}\text{O}_{\text{J3200}}(\text{NO}) = \Delta^{17}\text{O}(\text{HONO})$
J3201 $\text{HNO}_3 + \text{h}\nu \rightarrow \text{OH} + \text{NO}_2$	$\Delta^{17}\text{O}_{\text{J3201}}(\text{NO}_2) = \Delta^{17}\text{O}(\text{HNO}_3)$
J3202 $\text{HNO}_4 + \text{h}\nu \rightarrow 0.667\text{NO}_2 + 0.667\text{HO}_2 + 0.333\text{NO}_3 + 0.333\text{OH}$	$\Delta^{17}\text{O}_{\text{J3202}}(\text{NO}_2) = \Delta^{17}\text{O}(\text{HNO}_4 - \text{NO}_2)$ $\Delta^{17}\text{O}_{\text{J3202}}(\text{NO}_3) = 2/3 \Delta^{17}\text{O}(\text{HNO}_4 - \text{NO}_2) + 1/3 \Delta^{17}\text{O}(\text{HNO}_4 - \text{HO}_2)$

3.2.2 Case 2: explicit NO_x

In this case, the time evolution of $\Delta^{17}\text{O}$ of NO , NO_2 and NO_3 is computed explicitly. This means that the PSS approximation is not used at all regarding the computation of the $\Delta^{17}\text{O}$ of these species. Table 2 presents the chemical reactions for which the $\Delta^{17}\text{O}_i(\text{X})$ is different than in Case 1 (PSS NO_x).

The decomposition of N_2O_5 and HNO_4 through photolysis or thermal decomposition is treated as follows. Our base hypothesis is that the photolysis and thermal decomposition of HNO_4 proceed without scrambling of its isotopic composition upon dissociation. The case of N_2O_5 is more complex and is illustrated by Fig. 2. Upon dissociation or photolysis of N_2O_5 , the $\Delta^{17}\text{O}$ of NO_2 and NO_3 formed is given by the following equations, based on the assumption that the two N–O bonds of the dimer have an equal probability to break:

$$\begin{aligned} & \Delta^{17}\text{O}_{\text{N}_2\text{O}_5\text{decomp}}(\text{NO}_2) \\ &= 1/2 \times (\Delta^{17}\text{O}(\text{N}_2\text{O}_5 - \text{NO}_2) + \Delta^{17}\text{O}(\text{N}_2\text{O}_5 - \text{NO}_3)) \\ & \Delta^{17}\text{O}_{\text{N}_2\text{O}_5\text{decomp}}(\text{NO}_3) \\ &= 1/3 \times (\Delta^{17}\text{O}(\text{N}_2\text{O}_5 - \text{NO}_2) + 2 \times \Delta^{17}\text{O}(\text{N}_2\text{O}_5 - \text{NO}_3)) \end{aligned}$$

where $\Delta^{17}\text{O}(\text{N}_2\text{O}_5 - \text{NO}_2)$ and $\Delta^{17}\text{O}(\text{N}_2\text{O}_5 - \text{NO}_3)$ represent the $\Delta^{17}\text{O}$ of the two dimers making up N_2O_5 , i.e. NO_2 and NO_3 , respectively.

3.2.3 Case 3: explicit HO_x

In this case, in addition to the hypotheses of Case 2 (explicit NO_x), the $\Delta^{17}\text{O}$ value of HO_2 is allowed to vary in time and is computed explicitly. This also induces non-zero values of $\Delta^{17}\text{O}(\text{H}_2\text{O}_2)$, through reaction $\text{HO}_2 + \text{HO}_2$. Table 3 presents the chemical reactions for which the $\Delta^{17}\text{O}_i(\text{X})$ is different than in Case 1 (PSS NO_x) and 2 (explicit NO_x). Note that in Case 3 $\Delta^{17}\text{O}(\text{OH})$ is assigned a value of 0‰. Note that, strictly speaking, the O atoms in HO_2 are chemically not equivalent, because one is bonded to the H atom while the other one is not. This opens the possibility that the intramolecular distribution of $\Delta^{17}\text{O}$ within HO_2 is not statistically distributed, in a manner somewhat equivalent to ozone, as first noted by Savarino and Thiemens (1999b). For the sake of simplicity, we consider here that the $\Delta^{17}\text{O}$ of HO_2 can be represented as a single value, implicitly assuming that the intramolecular distribution of HO_2 is statistical.

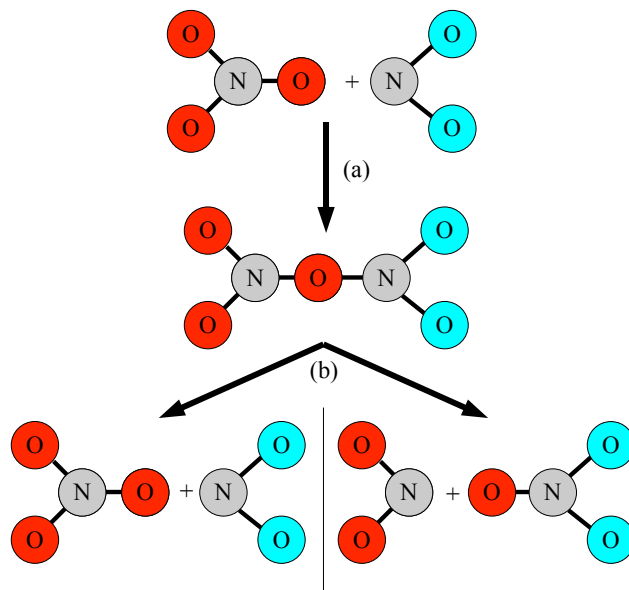


Fig. 2. Schematic illustrating the fate of oxygen atoms from NO_3 (in red) and NO_2 (in blue) during the formation (a) and decomposition (b) of N_2O_5 . Owing to the symmetry of the N_2O_5 molecule, the $\text{N}-\text{O}$ bonds are expected to have an equal probability to break upon thermal decomposition or photolysis. The $\Delta^{17}\text{O}$ of NO_2 formed upon this dissociation corresponds to the average between the $\Delta^{17}\text{O}$ of NO_2 and NO_3 making up N_2O_5 . The $\Delta^{17}\text{O}$ of NO_3 formed upon the dissociation of N_2O_5 is a slightly more complex function, due to the fact that in half cases two out of the three oxygen atoms of NO_3 initially stem from NO_2 , while one comes from the original NO_3 . See Sect. 3.2.2 for details.

3.2.4 Additional tests

In addition to the three main cases presented above, three additional tests were performed. They all are based on Case 3 (explicit NO_x and HO_x), i.e. they can all be independently compared to Case 3.

Case 4: NMDF $\text{H}+\text{O}_2$

In this case, we take into account that reaction $\text{H}+\text{O}_2 \rightarrow \text{HO}_2$ induces non-mass dependent fractionation of oxygen isotopes. The effect is assumed to be on the order of 1‰, according to Savarino and Thiemens (1999b). In practice, any HO_2 produced through this channel is thus attributed a $\Delta^{17}\text{O}$ value of 1‰.

Case 5: Scrambling upon the decomposition of HNO_4

In this case, it is assumed that the thermal decomposition and photolysis of HNO_4 induce a scrambling of its oxygen atoms. Table 4 presents the chemical reactions for which the $\Delta^{17}\text{O}_i(\text{X})$ is different than in Case 1 (PSS NO_x) for the species produced upon the thermal decomposition of HNO_4 .

Case 6: isotopic exchange between OH and H_2O

In this case, we take into account the isotopic exchange reaction between OH and H_2O :



where Q denotes one of the three O isotopes. This reaction leads to the erosion of $\Delta^{17}\text{O}(\text{OH})$ following isotopic exchange with water vapor, which has a 0‰ $\Delta^{17}\text{O}$. Tropospheric OH is always at photochemical steady-state during daytime given its extremely short lifetime (a few seconds at most). Under such conditions, its $\Delta^{17}\text{O}$ is computed as follows:

$$\Delta^{17}\text{O}(\text{OH}) = \frac{\sum_i L_i}{\sum_i L_i + k_{\text{R10}}[\text{OH}][\text{H}_2\text{O}]} \times \Delta^{17}\text{O}_{\text{OHsource}}(\text{OH}) \quad (14)$$

where values for k_{R10} were measured by Dubey et al. (1997). In this study, the sole chemical reaction considered inducing non-zero $\Delta^{17}\text{O}$ values in OH is the reaction between $\text{O}(^1\text{D})$ and H_2O . Mass-balance states that $\Delta^{17}\text{O}_{\text{OHsource}}(\text{OH}) = 1/2 \times \Delta^{17}\text{O}(\text{O}_3^*)$ (Morin et al., 2007). Under most conditions prevailing in the lower troposphere in mid-latitudes, $\Delta^{17}\text{O}(\text{OH}) = 0\text{‰}$ (Michalski et al., 2003). However, under cold conditions the isotopic exchange reaction can compete with its OH chemical sinks (Morin et al., 2007), which are mostly $\text{OH}+\text{CH}_4$ and $\text{OH}+\text{CO}$ (Finlayson-Pitts and Pitts, 2000). When Case 6 is tested, $\Delta^{17}\text{O}(\text{OH})$ is assigned a value calculated from Eq. (14) and the mixing ratio of CO, CH_4 and H_2O and the relevant kinetic rate constants.

3.3 Numerical implementation and computation of $\Delta^{17}\text{O}$

MECCA

The chemistry module MECCA (Model Efficiently Computing the Chemistry of the Atmosphere) is embedded in the CAABA (Chemistry As A Box-model Application) box-model (Sander et al., 2011). It uses an adaptative time resolution mathematical method to solve the stiff set of equations describing the evolution of the chemical composition of the portion of atmosphere hypothetically contained in a closed box.

Isotopic equations

The MECCA chemistry module, like all atmospheric chemistry models, solves the continuity equation for all considered species and all reactions simultaneously:

$$\frac{d}{dt}[\text{X}] = \sum_i P_i - \sum_j L_j$$

Considering that the model provides the necessary data at a time step t , it follows that at the next time step $t+\Delta t$:

$$[\text{X}](t+\Delta t) = [\text{X}](t) + \Delta t \times \sum_i P_i - \Delta t \times \sum_j L_j \quad (15)$$

Table 3. $\Delta^{17}\text{O}_i(\text{X})$ for Case 3: explicit NO_x and HO_x . Only equations featuring $\Delta^{17}\text{O}_i(\text{HO}_2)$ different from 0‰ are presented here.

Rxn #		$\Delta^{17}\text{O}_i(\text{X})$
G2104	$\text{OH} + \text{O}_3 \rightarrow \text{HO}_2 + \text{O}_2$	$\Delta^{17}\text{O}_{\text{G2104}}(\text{HO}_2) = 1/2 \times \Delta^{17}\text{O}(\text{O}_3^*)$
G2110	$2\text{HO}_2 \rightarrow \text{H}_2\text{O}_2 + \text{O}_2$	$\Delta^{17}\text{O}_{\text{G2110}}(\text{H}_2\text{O}_2) = \Delta^{17}\text{O}(\text{HO}_2)$
G2112	$\text{H}_2\text{O}_2 + \text{OH} \rightarrow \text{H}_2\text{O} + \text{HO}_2$	$\Delta^{17}\text{O}_{\text{G2112}}(\text{HO}_2) = \Delta^{17}\text{O}(\text{H}_2\text{O}_2)$
G3203	$\text{NO}_2 + \text{HO}_2 + (\text{M}) \rightarrow \text{HNO}_4$	$\Delta^{17}\text{O}_{\text{G3203}}(\text{HNO}_4 - \text{HO}_2) = \Delta^{17}\text{O}(\text{HO}_2)$
G3207	$\text{HNO}_4 + (\text{M}) \rightarrow \text{NO}_2 + \text{HO}_2$	$\Delta^{17}\text{O}_{\text{G3207}}(\text{HO}_2) = \Delta^{17}\text{O}(\text{HNO}_4 - \text{HO}_2)$
J3202	$\text{HNO}_4 + \text{h}\nu \rightarrow 0.667\text{NO}_2 + 0.667\text{HO}_2 + 0.333\text{NO}_3 + 0.333\text{OH}$	$\Delta^{17}\text{O}_{\text{J3202}}(\text{HO}_2) = \Delta^{17}\text{O}(\text{HNO}_4 - \text{HO}_2)$

Table 4. $\Delta^{17}\text{O}_i(\text{X})$ for Case 5: Scrambling upon thermal decomposition and photolysis of HNO_4

Rxn #		$\Delta^{17}\text{O}_i(\text{X})$
G3207	$\text{HNO}_4 + (\text{M}) \rightarrow \text{NO}_2 + \text{HO}_2$	$\Delta^{17}\text{O}_{\text{G3207}}(\text{NO}_2) = 1/2(\Delta^{17}\text{O}(\text{HNO}_4 - \text{NO}_2) + \Delta^{17}\text{O}(\text{HNO}_4 - \text{HO}_2))$ $\Delta^{17}\text{O}_{\text{G3207}}(\text{HO}_2) = 1/2(\Delta^{17}\text{O}(\text{HNO}_4 - \text{NO}_2) + \Delta^{17}\text{O}(\text{HNO}_4 - \text{HO}_2))$
J3202	$\text{HNO}_4 + \text{h}\nu \rightarrow 0.667\text{NO}_2 + 0.667\text{HO}_2 + 0.333\text{NO}_3 + 0.333\text{OH}$	$\Delta^{17}\text{O}_{\text{J3202}}(\text{NO}_2) = 1/2(\Delta^{17}\text{O}(\text{HNO}_4 - \text{NO}_2) + \Delta^{17}\text{O}(\text{HNO}_4 - \text{HO}_2))$ $\Delta^{17}\text{O}_{\text{J3202}}(\text{NO}_3) = 1/2(\Delta^{17}\text{O}(\text{HNO}_4 - \text{NO}_2) + \Delta^{17}\text{O}(\text{HNO}_4 - \text{HO}_2))$ $\Delta^{17}\text{O}_{\text{J3202}}(\text{HO}_2) = 1/2(\Delta^{17}\text{O}(\text{HNO}_4 - \text{NO}_2) + \Delta^{17}\text{O}(\text{HNO}_4 - \text{HO}_2))$

The same applies to the isotopic continuity equation (Eq. 2), so that:

$$[\text{X}](t + \Delta t) \times \Delta^{17}\text{O}(\text{X})(t + \Delta t) = [\text{X}](t) \times \Delta^{17}\text{O}(\text{X})(t) \quad (16)$$

$$+ \Delta t \times \sum (P_i \times \Delta^{17}\text{O}_i(\text{X})(t)) - \Delta t \times (\sum_j L_j) \times \Delta^{17}\text{O}(\text{X})(t)$$

By combining Eqs. (15) and (3.3), $\Delta^{17}\text{O}(\text{X})(t + \Delta t)$ can be inferred as a function of the relevant chemical and isotopic data at time t . This simple explicit approach was implemented in a computer program separate from MECCA, which takes as input a data file containing the variables dealt with in Eqs. (15) and (3.3) at each time step, and processes them according to the different cases described above in terms of $\Delta^{17}\text{O}_i(\text{X})$ to compute the time evolution of $\Delta^{17}\text{O}$ of each relevant species.

One major issue that has to be considered when using this simple approach pertains to the comparison of the chemical lifetime of a species X and the time-step of the integration of Eqs. (15) and (3.3). Indeed, if the lifetime of X is shorter than the time step considered, then the total chemical production or destruction during a given time step Δt may exceed the amount of species X dealt with in the box (or grid-cell). This causes immediate failure of the integration procedure. The time step of the isotopic calculations performed here was chosen accordingly. A time resolution of 10 s was found to be sufficient to avoid integration issues such as described above. More integrated approaches, fully embedded into the box-model itself, have been developed and avoid such shortcomings (see e.g., Gromov et al., 2010). However, for the sake of

the present study, and taking advantage of the easiness of manipulating $\Delta^{17}\text{O}$ through simple mass-balance equations, we preferred the implementation presented above for this study.

3.4 Presentation of MECCA model runs

Our base-run corresponds to atmospheric settings typical of the remote, mid-latitude (45°N) boundary layer during springtime. Photolysis rate coefficients are calculated by the model (Sander et al., 2005). The model run is started on 1 April, at a temperature of 293 K, a relative humidity of 81%, with a starting NO_2 mixing ratio of 20 pmol mol^{-1} . Initial values for the mixing-ratio of main atmospheric species follow: CH_4 , $1.8 \mu\text{mol mol}^{-1}$; CO , 70 nmol mol^{-1} ; H_2O_2 , $600 \text{ pmol mol}^{-1}$; HNO_3 , 5 pmol mol^{-1} ; HCHO , 30 pmol mol^{-1} ; O_3 , 25 nmol mol^{-1} . The model accounts for dry deposition of NO_2 , HNO_3 , N_2O_5 and H_2O_2 . In contrast, no emissions into the model box are considered during the model run. After a spin-up time of 1 day, sufficient to initialize the mixing ratio of short-lived species, the time evolution of the mixing ratio and isotope anomaly of short-lived species is analyzed during 36 h, corresponding to the time frame between 24 and 60 h from the start of the model run. In lack of emissions of primary species into the box considered, this suffices to identify and study the main features of the diurnal variations of the mixing ratio and $\Delta^{17}\text{O}$ of short-lived species while not suffering from the inherent limitations of box-modeling experienced when longer time periods are considered (Sander et al., 2005).

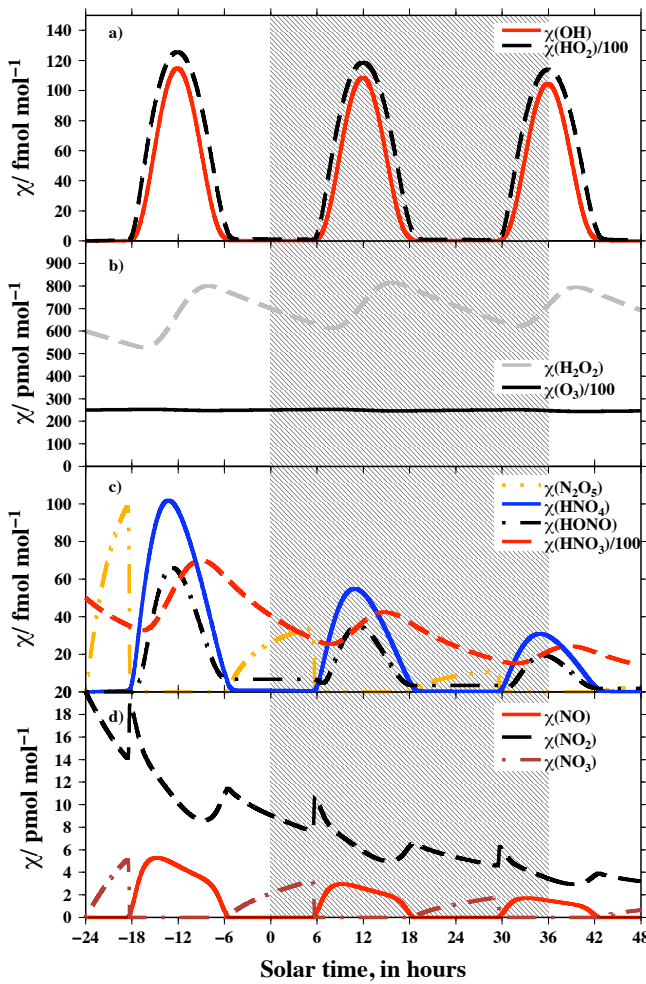


Fig. 3. Time series of the mixing ratio (χ) of the main atmospheric species studied, for the base model run ($T=293\text{ K}$, 45° N , see Sect. 3.4 for details). (a) OH and HO_2 , (b) O_3 and H_2O_2 , (c) N_2O_5 , HNO_4 , HONO , (d) NO , NO_2 and NO_3 . The shaded area represents the time period used in the rest of article for the isotopic discussion.

We concentrate our in-depth analysis on this one model run, which shows many different interesting features of the diurnal variations of $\Delta^{17}\text{O}$ of short-lived species and their sensitivity of the various assumptions tested through Cases 1 to 6. The intricacy and the highly non-linear coupling between HO_x and NO_x including their $\Delta^{17}\text{O}$ requires careful attention to decipher the causes for the variation of $\Delta^{17}\text{O}$. The relevance of the conclusions reached from this analysis is assessed using other model runs undertaken under different atmospheric conditions. Indeed, atmospheric chemical processes depend in particular on temperature, time of the year and latitude (through their control of incoming solar radiation) and the chemical regime of the atmosphere.

4 Results

4.1 Description and analysis of the base model run

4.1.1 Diurnal variations in mixing ratios and reaction rates

Figure 3 shows the evolution of the mixing ratio of O_3 , HO_x and NO_x/NO_y (NO_y refers to sum of NO_x and its reservoir species: NO_3 , N_2O_5 , HONO , HNO_3 , HNO_4) simulated by MECCA under the conditions of the base model run presented in Sect. 3.4. Negative time corresponds to the above-mentioned spin-up time period. Note that the time axis is the same for all the plots exhibiting time series in this article. The model results show typical variations in the mixing ratio of the species of interest, notably with peak values of OH, HO_2 and NO reached during the day. The NO_x/NO_y partitioning changes diurnally, with species such as NO_3 and N_2O_5 present mostly during the night, and species such as HNO_4 , HONO present mostly during the day. H_2O_2 is produced during the day, and undergoes dry deposition which leads to a reduction of its mixing ratio during the night. The mixing ratio of ozone remains quasi-constant during the time period studied, illustrating that the simulation reproduces the chemical steady-state prevailing in the remote, mid-latitude boundary layer.

As a straightforward corollary of the above paragraph, it appears that in this simulation the $\text{OH}+\text{NO}_2$ and HNO_4 hydrolysis are mostly daytime nitrate production pathways, while NO_3+RH and N_2O_5 hydrolysis proceed only at night, when significant amounts of NO_3 and N_2O_5 are present. Note that this study does not aim at disentangling complex aspects of the daytime chemistry of N_2O_5 revealed by recent field campaigns (e.g., Brown et al., 2006). H_2O_2 is only produced during the day, when HO_2 maximizes. Figure 4 exemplifies such opposed behavior and illustrates the concept behind diurnally-integrated isotopic signature (DIIS) of the nitrate and hydrogen peroxide sources. From the analysis of this figure, it appears obvious that the nighttime $\Delta^{17}\text{O}$ values of HO_2 have no impact on the $\Delta^{17}\text{O}$ of H_2O_2 produced. Only daytime $\Delta^{17}\text{O}$ values are worth discussing in this case.

4.1.2 Overview of the diurnally-integrated isotopic signatures (DIIS) values for atmospheric nitrate and hydrogen peroxide sources

Table 5 shows the DIIS ($\overline{\Delta^{17}\text{O}_i(\text{NO}_3^-)}$) values for the four atmospheric nitrate sources considered, as well as for H_2O_2 . The main results of this simulation are that

- $\Delta^{17}\text{O}_{\text{OH}+\text{NO}_2}(\text{NO}_3^-)$ values are on the order of 20‰ and do not seem significantly dependent to within 0.1‰ upon the different isotopic assumptions tested, except Case 5 (Isotopic scrambling during thermal decomposition and photolysis of HNO_4) which is detailed below. In particular, whether $\Delta^{17}\text{O}(\text{NO}_2)$ is computed

Table 5. Diurnally-integrated isotopic signature (DIIS) values for the atmospheric nitrate and H_2O_2 production channels, respectively (in ‰ units). Overview of the results from the base model run carried out in springtime (1 April) under mid-latitude (45°N) remote boundary layer conditions.

	$\text{OH} + \text{NO}_2$	$\text{NO}_3 + \text{RH}$	$\text{N}_2\text{O}_5\text{hydrol}$	$\text{HNO}_4\text{hydrol}$	H_2O_2
Case 1 – NO_x PSS	20.3	42.6	35.1	15.7	0.0
Case 2 – NO_x explicit	20.4	40.2	33.2	15.7	0.0
Case 3 – HO_x explicit	20.5	40.2	33.3	16.3	1.1
Case 4 – MIF in $\text{H} + \text{O}_2$	20.5	40.2	33.3	16.7	1.8
Case 5 – Scrambling of HNO_4	19.7	38.0	31.2	16.0	1.5
Case 6 – $\text{OH} + \text{H}_2\text{O}$ isotopic exchange	20.5	40.2	33.3	16.3	1.1

explicitly or using the PSS formula has no impact on the DIIS value. This shows that, to compute the DIIS of this reaction channel, it is correct to use the PSS formalism to calculate $\Delta^{17}\text{O}(\text{NO}_2)$. This stems from the fact that, when $\Delta^{17}\text{O}(\text{NO}_2)$ deviates from its PSS value, i.e. during the night, the $\text{OH} + \text{NO}_2$ reaction is ineffective owing to the simultaneous absence of OH. Thus, PSS $\Delta^{17}\text{O}(\text{NO}_2)$ values can be used to compute the DIIS of this reaction channel, as long as they are correctly scaled with the strength of the $\text{OH} + \text{NO}_2$ reaction.

- $\Delta^{17}\text{O}_{\text{HNO}_4\text{hydrol}}(\text{NO}_3^-)$ values are on the order of 16‰ and do not depend on the method to compute the $\Delta^{17}\text{O}$ of NO_x (Case 1 (PSS NO_x) and Case 2 (explicit NO_x) yield similar results). When $\Delta^{17}\text{O}(\text{HO}_2)$ is computed explicitly, $\Delta^{17}\text{O}_{\text{HNO}_4\text{hydrol}}(\text{NO}_3^-)$ values increase moderately by ca. 0.6‰.
- $\Delta^{17}\text{O}_{\text{NO}_3+\text{RH}}(\text{NO}_3^-)$ and $\Delta^{17}\text{O}_{\text{N}_2\text{O}_5\text{hydrol}}(\text{NO}_3^-)$ are on the order of 40 and 33.5‰, respectively, and show a significant difference between Case 1 (PSS NO_x and Case 2 (explicit NO_x), i.e. whether PSS is used to compute the $\Delta^{17}\text{O}$ of NO_x and NO_y . Using the PSS formulation for NO_x yields an overestimation on the order of 2‰ of the DIIS values for both these nitrate production channels.
- $\Delta^{17}\text{O}_{\text{HO}_2+\text{HO}_2}(\text{H}_2\text{O}_2)$ values are 0 for both Cases 1 and 2 (PSS and explicit NO_x , respectively), consistent with the fact that $\Delta^{17}\text{O}(\text{HO}_2)$ is assigned a value of 0. When $\Delta^{17}\text{O}(\text{HO}_2)$ is computed explicitly, the $\Delta^{17}\text{O}_{\text{HO}_2+\text{HO}_2}(\text{H}_2\text{O}_2)$ reaches 1.1‰ (Case 3, explicit NO_x and HO_x). Taking into account non-mass dependent fractionation (NMDF) of 1‰ in the $\text{H} + \text{O}_2$ reaction leads to increasing the $\Delta^{17}\text{O}_{\text{HO}_2+\text{HO}_2}(\text{H}_2\text{O}_2)$ value by 0.7‰.
- under the environmental conditions tested, whether isotopic exchange between OH and H_2O is considered has no significant impact on all the reaction pathways considered. This simply indicates that $\Delta^{17}\text{O}(\text{OH})=0\%$ under these environmental conditions.

– Isotopic scrambling during the thermal and photolytical decomposition of and HNO_4 leads to lowering the DIIS value of all reaction pathways, except for H_2O_2 production.

4.1.3 Detailed analysis of the main results

Representation of diurnal variations of $\Delta^{17}\text{O}(\text{NO}_2)$

As shown on Fig. 4a, $\Delta^{17}\text{O}(\text{NO}_2)$ exhibits diurnal variations with a maximum during the night and a minimum during the day, consistent with previous expectations (Morin, 2009). Figure 5 compares the results obtained using permanent photochemical steady-state (Case 1, NO_x PSS) and explicitly computed (Case 2, NO_x explicit, see Sect. 3.2.2). During the day, both calculations show a minimum at noon, on the order of 28‰. This is explained by the fact that during the day, the contribution of the $\text{NO} + \text{RO}_2$ and $\text{NO} + \text{HO}_2$ to the production of NO_2 peaks at noon, when peroxy radicals reach their maximum values (see Fig. 3). Owing to the short lifetime of NO_2 during the day, the result of the computation based on PSS is fully consistent with the explicit computation. This explains why $\Delta^{17}\text{O}_{\text{OH}+\text{NO}_2}(\text{NO}_3^-)$ is the same under Case 1 and Case 2 (PSS and explicit NO_x , respectively, see Table 5), because this pathway operates only during the day, when $\Delta^{17}\text{O}(\text{NO}_2)$ has the same value in both cases.

The major difference between the two simulations occurs at night. Indeed, while the result from PSS leads $\Delta^{17}\text{O}(\text{NO}_2)$ to reach values above 41‰ at night (i.e., on the order of $\Delta^{17}\text{O}_{\text{NO}+\text{O}_3}(\text{NO}_2)$), the result from the explicit calculation does not exceed 39‰ at night, except for a limited period of time at dawn. The explanation for this behavior follows: at dusk, the $\Delta^{17}\text{O}(\text{NO}_2)$ is fixed by the PSS conditions which prevail just before PSS recycling of NO_x becomes insignificant. At this point, NO_2 becomes relatively inert and its $\Delta^{17}\text{O}$ does not vary anymore. As evidenced by Fig. 5, nighttime $\Delta^{17}\text{O}(\text{NO}_2)$ corresponds to the $\Delta^{17}\text{O}(\text{NO}_2)$ value computed at PSS when the lifetime of NO_2 is on the order of 10 min. It is then “frozen” until the dawn comes, along with the restart of photochemical activity. The difference between the two calculations lies between 2 and 3‰ under the conditions of the base model run. This explains why DIIS values for the

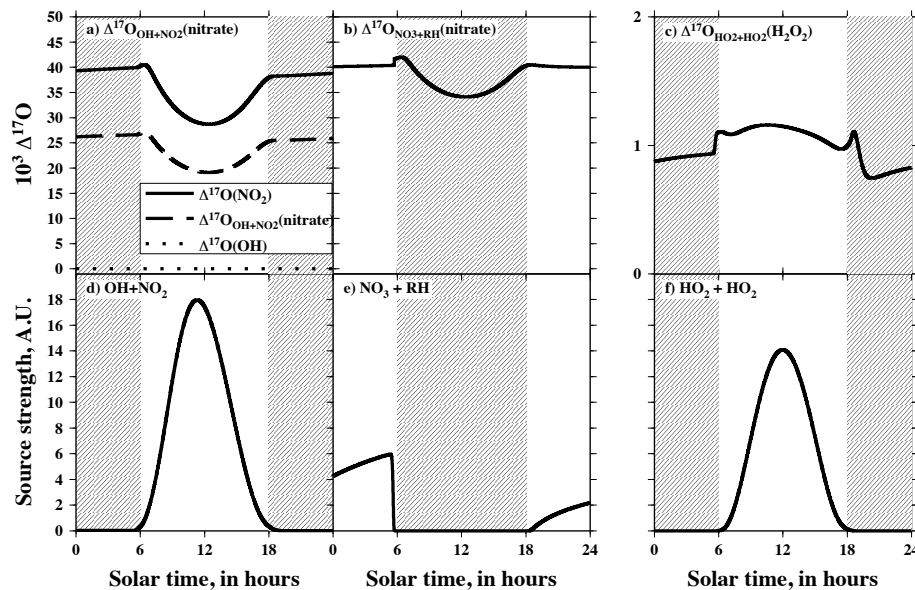


Fig. 4. Simulated diurnal variations of the isotopic signature $\Delta^{17}\text{O}_i(\text{nitrato})$ and $\Delta^{17}\text{O}_i(\text{H}_2\text{O}_2)$ (**a–c**) and the strength (**d–f**) of the $\text{OH}+\text{NO}_2$, NO_3+RH nitrate production channel and H_2O_2 production channel, respectively. Note that in the case of the $\text{OH}+\text{NO}_2$ reaction, the $\Delta^{17}\text{O}$ values of individual precursors (OH and NO_2) are shown along with the isotopic signature of this reaction channel (see Sect. 2.4.1). Results originate from the base model run ($T=293\text{ K}$, 45° N , see Sect. 3.4 for details) under the isotopic hypotheses of Case 3 (explicit NO_x and HO_x). Hatched areas represent the period of the day when the considered reaction pathway proceeds insignificantly, thus the corresponding $\Delta^{17}\text{O}$ which could then be transferred to the reaction products is irrelevant. The diurnally-integrated isotopic source (DIIS) values correspond to the average of values from the upper panel, weighted by the values of the lower one. Note that the strength of the production pathways are expressed in arbitrary units different in each cases, thus the panels (**d**) to (**f**) cannot be directly compared.

Table 6. Diurnally-integrated source isotopic signature (DIIS) for the four nitrate and H_2O_2 production channels considered (in ‰ units). Overview of the results from three model runs carried out at different periods of the year (W=1 January, Sp.=1 April and Su.=1 July, respectively), under mid-latitude (45° N) remote boundary layer conditions.

	$\text{OH}+\text{NO}_2$			NO_3+RH			$\text{N}_2\text{O}_5\text{hydrol}$			$\text{HNO}_4\text{hydrol}$			H_2O_2		
	W	Sp.	Su.	W	Sp.	Su.	W	Sp.	Su.	W	Sp.	Su.	W	Sp.	Su.
Case 1 – NO_x PSS	24.9	20.3	17.3	42.7	42.6	42.3	35.2	35.1	34.9	18.8	15.7	13.6	0.0	0.0	0.0
Case 2 – NO_x explicit	24.9	20.4	17.3	40.7	40.2	39.8	33.8	33.2	32.8	18.8	15.7	13.6	0.0	0.0	0.0
Case 3 – HO_x explicit	24.9	20.5	17.4	40.8	40.2	39.8	33.8	33.3	32.8	19.4	16.3	14.2	1.1	1.1	1.0
Case 4 – MIF in $\text{H}+\text{O}_2$	25.0	20.5	17.5	40.8	40.2	39.8	33.8	33.3	32.8	19.8	16.7	14.6	1.8	1.8	1.7
Case 5 – Scrambling of HNO_4	24.2	19.7	16.7	38.0	38.0	38.0	31.4	31.2	31.0	19.9	16.0	13.7	2.9	1.5	1.1
Case 6 – $\text{OH}+\text{H}_2\text{O}$ isotopic exchange	25.1	20.5	17.5	40.8	40.2	39.8	33.8	33.3	32.8	19.4	16.3	14.2	1.1	1.1	1.0

nighttime nitrate production pathways depend strongly on the method chosen to compute $\Delta^{17}\text{O}(\text{NO}_x)$ and $\Delta^{17}\text{O}(\text{NO}_y)$, because much of the difference occurs at night.

$\Delta^{17}\text{O}(\text{HO}_2)$ and $\Delta^{17}\text{O}(\text{H}_2\text{O}_2)$

In Cases 3, 4, 5 and 6, where $\Delta^{17}\text{O}(\text{HO}_2)$ is computed explicitly, non-zero $\Delta^{17}\text{O}(\text{HO}_2)$ values are found. Figure 6 shows the diurnal variations of $\Delta^{17}\text{O}(\text{HO}_2)$ and $\Delta^{17}\text{O}(\text{H}_2\text{O}_2)$. The non-zero $\Delta^{17}\text{O}$ value in Case 3 (explicit NO_x and HO_x , on the order of 1‰, stems directly from the $\text{OH}+\text{O}_3$ reaction producing HO_2 with a non-zero $\Delta^{17}\text{O}$ value, which is then mixed with other sources of HO_2 .

The addition of non-mass dependent fractionation through the $\text{H}+\text{O}_2$ reaction, which is the dominant HO_2 production reaction, results in elevating the $\Delta^{17}\text{O}(\text{HO}_2)$ value by roughly the magnitude of the isotopic fractionation constant. Combining the explicit calculation of the time evolution of $\Delta^{17}\text{O}(\text{HO}_2)$ with the inclusion of non-mass dependent fractionation occurring during the $\text{H}+\text{O}_2$ reaction leads to daytime $\Delta^{17}\text{O}(\text{HO}_2)$ values on the order of 2‰.

We note that the corresponding $\Delta^{17}\text{O}_{\text{HO}_2+\text{HO}_2}(\text{H}_2\text{O}_2)$ values for either Case 3 or 4 (explicit NO_x and HO_x and NMDF $\text{H}+\text{O}_2$, respectively), 1.1 and 1.8‰, respectively, are consistent with the experimental results of Savarino and Thiemens (1999a), who measured rainwater $\Delta^{17}\text{O}(\text{H}_2\text{O}_2)$

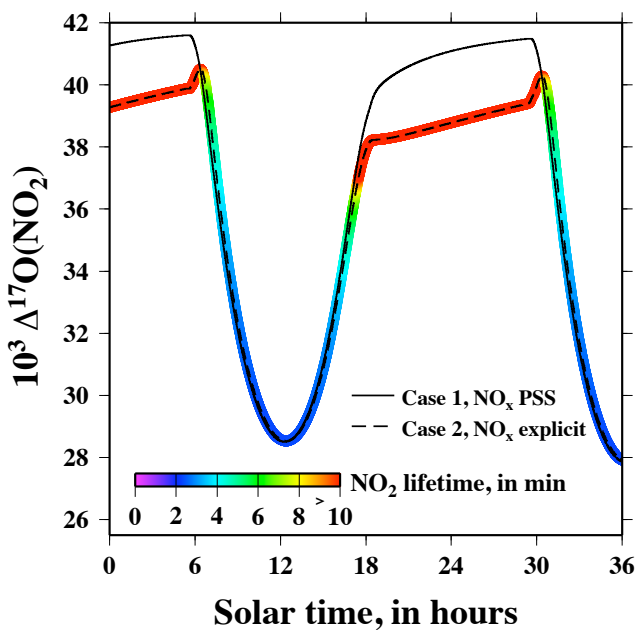


Fig. 5. Diurnal variation of $\Delta^{17}\text{O}(\text{NO}_2)$ calculated using two different approaches, i.e. permanent photochemical steady-state for NO_x (Case 1, solid line) and the explicit computation of $\Delta^{17}\text{O}(\text{NO}_x)$ (Case 2, dashed line). The dashed line representing the results of the simulations under Case 2 is overlaid with a color code exhibiting the diurnal variation of the photolytical lifetime of NO_2 . All values above 10 min are shown in red (at night, the photochemical lifetime of NO_2 is virtually infinite).

values ranging between 0.9 and 2.0‰, under coastal conditions in California.

Impact of isotopic scrambling during the thermal and photolytical decomposition of HNO_4

Case 5 tests the hypothesis where thermal decomposition and photolysis leads to isotopic scrambling between O atoms in molecules making up HNO_4 (see Table 4). Under such conditions, it is observed that the $\Delta^{17}\text{O}$ of HO_2 increases, while $\Delta^{17}\text{O}$ of NO_x generally decreases. This behavior is reflected in the DIIS values of the relevant reactions (see Table 5). Detailed investigation of the reasons for this result reveals that much of the effect proceeds through the thermal decomposition of HNO_4 , especially at dusk when HNO_4 thermal decomposition is on the order of its formation rate due to reduced photochemical activity lowering the amount of HO_2 . Through slow but steady cycles of formation/decomposition, HNO_4 temporarily bridges the pool of oxygen atoms within NO_x and HO_x , leading to lowering the $\Delta^{17}\text{O}$ of NO_x and increasing the $\Delta^{17}\text{O}$ of HO_x in a significant manner (see Fig. 6). In the following, we do not further discuss the impact of the hypothesis of Case 5, although model results are also given for this case.

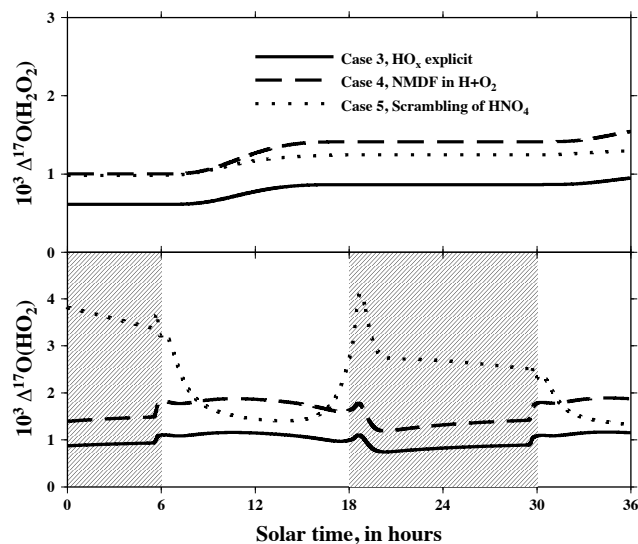


Fig. 6. Simulated diurnal variations of $\Delta^{17}\text{O}(\text{H}_2\text{O}_2)$ (top) and $\Delta^{17}\text{O}(\text{HO}_2)$ (bottom) under the various hypotheses tested, from the results of the base model run. Note that in Case 1 and 2 (PSS and explicit NO_x), $\Delta^{17}\text{O}(\text{HO}_2)$ is set to 0. The hatched area covers night-time periods when the presence of HO_2 in the atmosphere is insignificant, hence the relevance of its $\Delta^{17}\text{O}$ value.

4.2 Sensitivity to atmospheric conditions

This section presents the results obtained under different conditions than in the base model run. For the sake of brevity, and since the physico-chemical reasons behind the observed behavior are similar to the phenomena described above, we focus our attention on DIIS values, which provide an efficient metric to compare model runs carried out under different environmental conditions.

4.2.1 Impact of seasonal variations

Using the same chemical mechanism and the same initial chemical composition of the boundary layer, model runs were performed at different times of the year, i.e. starting from 1 January with a temperature of 283 K and 1 July with a temperature of 303 K to see whether seasonal variations in environmental conditions (temperature and actinic flux) can modify the conclusions reached above for the springtime model run, started on 1 April with a temperature of 293 K. The photochemical activity increases monotonically from the winter to summer model runs, as expected (chemical data not shown).

The model shows that the DIIS of daytime nitrate production channels ($\Delta^{17}\text{O}_{\text{OH}+\text{NO}_2}(\text{NO}_3^-)$ and $\Delta^{17}\text{O}_{\text{HNO}_4\text{hydrol}}(\text{NO}_3^-)$) are most dependent on the season, due to their strong ties to photochemical activity, which controls $\Delta^{17}\text{O}$ of NO_2 and HNO_4 through photochemical steady state during the day. The $\Delta^{17}\text{O}_{\text{OH}+\text{NO}_2}(\text{NO}_3^-)$ varies

Table 7. Comparison of diurnally-integrated source isotopic signature (DIIS, in ‰ units) for the four nitrate and H_2O_2 production channels considered under mid-latitude (45°N , 293 K) and Arctic (80°N , 253 K) conditions in springtime (1 April).

	OH+ NO_2		NO ₃ +RH		N ₂ O ₅ hydrol		HNO ₄ hydrol		H ₂ O ₂	
	45° N	80° N	45° N	80° N	45° N	80° N	45° N	80° N	45° N	80° N
Case 1 – NO _x PSS	20.3	26.0	42.6	42.1	35.1	34.4	15.7	19.6	0.0	0.0
Case 2 – NO _x explicit	20.4	25.9	40.2	41.1	33.2	33.6	15.7	19.5	0.0	0.0
Case 3 – HO _x explicit	20.5	25.9	40.2	41.1	33.3	33.6	16.3	19.9	1.1	0.8
Case 4 – MIF in H+O ₂	20.5	26.0	40.2	41.1	33.3	33.7	16.7	20.3	1.8	1.6
Case 5 – Scrambling of HNO ₄	19.7	24.9	38.0	36.2	31.2	28.5	16.0	21.1	1.5	3.8
Case 6 – OH+H ₂ O isotopic exchange	20.5	28.1	40.2	41.1	33.3	33.6	16.3	20.0	1.1	0.9

significantly, from ca. 17‰ in summer to ca. 25‰ during the winter. $\Delta^{17}\text{O}_{\text{HNO}_4\text{hydrol}}(\text{NO}_3^-)$ also varies, from ca. 14‰ in summer to ca. 19‰ in winter.

In contrast, the DIIS of nighttime nitrate production channels exhibits a stronger dependence upon the isotopic assumption (as detailed in Sect. 4.1.3), but shows little seasonal variations. The biggest variation is between Case 1 (PSS NO_x) and Case 2 (explicit NO_x), the former leading to an overestimation ranging from 1.5 to 2.0‰, from winter to summer for both N₂O₅ hydrolysis and NO₃+RH. The $\Delta^{17}\text{O}_{\text{NO}_3+\text{RH}}(\text{NO}_3^-)$ and $\Delta^{17}\text{O}_{\text{N}_2\text{O}_5\text{hydrol}}(\text{NO}_3^-)$ both vary within about 1‰ seasonally, and remain on the order of 40 and 33‰ year-round, respectively.

Last, $\Delta^{17}\text{O}_{\text{HO}_2+\text{HO}_2}$ (H₂O₂) values show little seasonal variation (less than 0.1‰). They remain consistently on the order of 1‰ when only the OH+O₃ reaction is responsible for $\Delta^{17}\text{O}$ transfer from O₃ to HO₂. They increase to around 1.7‰ when non-mass dependent fractionation of 1‰ is considered throughout the reaction H+O₂ → HO₂. The only major change occurs in Case 5, i.e. considering scrambling during the thermal decomposition and photolysis of HNO₄.

Under the conditions experienced for our base model run, the isotopic exchange reaction between OH and H₂O does not lead to $\Delta^{17}\text{O}(\text{OH})$ values significantly different from 0. This explains why the DIIS values for Case 6 (OH+H₂O isotopic exchange) are very similar to that of Case 3 (explicit NO_x and HO_x). This effect becomes significant only at lower temperatures (see Morin et al., 2007) and is further explored in Sect. 4.2.2.

4.2.2 Higher latitude and colder conditions

A simulation was carried out under springtime Arctic conditions, i.e. a latitude of 80°N and temperature of 253 K, starting from 1 April. The results of this comparison is shown in terms of DIIS values in Table 7.

The DIIS values of daytime nitrate production channels show a strong difference between Arctic and mid-latitude conditions. With the exception of Case 6 (OH+H₂O isotopic exchange), the Arctic $\Delta^{17}\text{O}_{\text{OH}+\text{NO}_2}(\text{NO}_3^-)$ values are ca. 5.5‰ higher than at mid-latitudes, which simply stems

from reduced photochemical recycling under reduced insulation prevailing in the Arctic and colder temperatures. It is noteworthy that under Arctic conditions, owing to the lower temperatures prevailing, the value of $\Delta^{17}\text{O}_{\text{OH}+\text{NO}_2}(\text{NO}_3^-)$ is 2‰ higher under Case 6 (OH+H₂O isotopic exchange) than under other cases (except Case 5). The diurnal variations of $\Delta^{17}\text{O}(\text{NO}_2)$ is similar for Case 2 (explicit NO_x) and Case 6 (OH+H₂O isotopic exchange) under Arctic conditions, demonstrating that all of the difference observed stems from the fact that $\Delta^{17}\text{O}(\text{OH})$ amounts ca. 6‰ under Arctic conditions and Case 6, consistent with the initial estimates provided by Morin et al. (2007).

The values of $\Delta^{17}\text{O}_{\text{NO}_3+\text{RH}}(\text{NO}_3^-)$ and $\Delta^{17}\text{O}_{\text{N}_2\text{O}_5\text{hydrol}}(\text{NO}_3^-)$ are very similar under mid-latitude and Arctic conditions, on the order of 40.5‰ and 33.5‰, respectively. Note also that the impact of the hypothesis of Case 6 (OH+H₂O isotopic exchange) on the DIIS values is insignificant. Arctic values of $\Delta^{17}\text{O}_{\text{HO}_2+\text{HO}_2}$ (H₂O₂) tend to be a little lower by a few tenths of ‰. The effect of Case 6 is limited to 0.1‰ in terms of $\Delta^{17}\text{O}_{\text{HO}_2+\text{HO}_2}$ (H₂O₂).

In summary, the impact of colder and more boreal environmental conditions is mostly seen for the DIIS of daytime nitrate production, upon which photochemical conditions and the $\Delta^{17}\text{O}$ of OH have a direct impact. The DIIS of nighttime nitrate production channels as well as H₂O₂ seem to be fairly insensitive to these factors.

4.2.3 Higher initial NO_x mixing ratio

A further simulation was carried out under springtime mid-latitude conditions (45°N , 293 K), with an initial NO_x mixing ratio of 2 nmol mol⁻¹ instead of 20 pmol mol⁻¹ in the base run. The results in terms of DIIS are shown in Table 8. The impact of performing the PSS approximation to compute $\Delta^{17}\text{O}$ of NO_x is similar, i.e. there is no impact on daytime nitrate production pathways and H₂O₂. It is more visible in the case of nighttime nitrate production pathways, although the difference between Case 1 (PSS NO_x) and Case 2 (explicit NO_x) for nighttime nitrate production pathways is smaller than under the conditions of the base model run.

Table 8. Comparison of diurnally-integrated source isotopic signature (DIIS, in ‰ units) for the four nitrate and H_2O_2 production channels considered, respectively under mid-latitude (45°N , 293 K) and under starting NO_x levels of 20 pmol mol^{-1} (base) and 2 nmol mol^{-1} (high NO_x) in springtime (1 April).

	OH+NO ₂		NO ₃ +RH		N ₂ O ₅ hydrol		HNO ₄ hydrol		H ₂ O ₂	
	base	high NO _x	base	high NO _x	base	high NO _x	base	high NO _x	base	high NO _x
Case 1 – NO _x PSS	20.3	17.3	42.6	42.1	35.1	34.4	15.7	17.5	0.0	0.0
Case 2 – NO _x explicit	20.4	17.3	40.2	41.1	33.2	33.6	15.7	17.5	0.0	0.0
Case 3 – HO _x explicit	20.5	17.4	40.2	41.1	33.3	33.6	16.3	18.2	1.1	1.3
Case 4 – MIF in H + O ₂	20.5	17.5	40.2	41.1	33.3	33.7	16.7	18.5	1.8	1.9
Case 5 – Scrambling of HNO ₄	19.7	16.7	38.0	36.2	31.2	28.5	16.0	19.7	1.5	4.5
Case 6 – OH+H ₂ O isotopic exchange	20.5	17.5	40.2	41.1	33.3	33.6	16.3	18.2	1.1	1.3

Table 9. Comparison between the DIIS values for OH+NO₂ and NO₃+RH with the corresponding values assigned to these reactions by Alexander et al. (2009), in ‰ units. The values deduced from the algorithm presented by Alexander et al. (2009) are compared to DIIS values computed using Cases 1 and 3, under the conditions of the base model run (mid-latitudes).

	OH+NO ₂		NO ₃ +RH	
	this study	Alexander et al. (2009)	this study	Alexander et al. (2009)
Case 1 – NO _x PSS	20.3	19.3	42.6	42.6
Case 3 – HO _x and NO _x explicit	20.5		40.2	

Due to enhanced photochemical activity fueled by higher initial NO_x levels, the $\Delta^{17}\text{O}_{\text{OH}+\text{NO}_2}(\text{NO}_3^-)$ values are reduced by 3‰ when higher initial NO_x levels are set. The impact on nighttime nitrate production channels is limited, with $\Delta^{17}\text{O}_{\text{NO}_3+\text{RH}}(\text{NO}_3^-)$ and $\Delta^{17}\text{O}_{\text{N}_2\text{O}_5\text{hydrol}}(\text{NO}_3^-)$ values on the order of 40.5‰ and 34‰, respectively, varying about 1‰ across this strong chemical gradient.

5 Discussion and implications

5.1 Implications for modeling $\Delta^{17}\text{O}(\text{NO}_3^-)$

We compare here our results to the implementation of $\Delta^{17}\text{O}(\text{NO}_3^-)$ into the GEOS-Chem chemistry transport model, which was recently carried out by Alexander et al. (2009). In this work, $\Delta^{17}\text{O}(\text{NO}_x)$ was computed under the hypothesis of photochemical steady-state. For the sole daytime nitrate production channel considered (OH+NO₂), $\Delta^{17}\text{O}(\text{NO}_2)$ was estimated using the α value (see Sect. 3.2.1) computed using accumulated reaction rates between 10:00 and 14:00 solar time. For nighttime nitrate production channels, Alexander et al. (2009) used the photochemical steady-state formalism using NO₂ production rates accumulated between 00:00 and 02:00 solar time. We compute the $\Delta^{17}\text{O}$ inherited by atmospheric nitrate through the OH+NO₂ and NO₃+RH using the algorithm of Alexander et al. (2009) presented above, and compare it to the corresponding DIIS val-

ues. The results are given in Table 9. We find that the algorithm introduced by Alexander et al. (2009) underestimates the isotopic signature of the OH+NO₂ channel by 1‰ under springtime conditions, because it ignores contributions of this channel before 10:00 and after 14:00, when $\Delta^{17}\text{O}(\text{NO}_2)$ is relatively higher than during noontime but the OH+NO₂ reaction proceeds significantly. The underestimates ranges between 0.5 and 1.5‰ when the comparison extends to other seasons and latitudes considered in the model runs. Alexander et al. (2009) also overestimate the isotopic signature of the NO₃+RH channel by 1.6‰, due to the fact that they use PSS equations to derive $\Delta^{17}\text{O}(\text{NO}_y)$ at night, which has been proven above to cause significant overestimation of the DIIS of nighttime nitrate production channels.

We strongly suggest that DIIS values are implemented in large-scale modeling frameworks, such as GEOS-Chem, to avoid performing such errors. To facilitate this, we provide below a method to implement this concept within a model such as GEOS-Chem, using the formalism of Alexander et al. (2009). The method is independent of the choice of $\Delta^{17}\text{O}(\text{O}_3)$ although they are based on the hypothesis that $\Delta^{17}\text{O}(\text{O}_3)$ remains constant throughout the day. Indeed, as an alternative to DIIS values introduced in Sect. 2.4.1 above, we introduce here the concept of *effective α* values, as follows. We combine Eqs. (6), (7) and (8) with the $\Delta^{17}\text{O}$ transfer functions under photochemical steady-state conditions, described in Sect. 3.2.1. During the day, at PSS, the isotopic signature of NO₂+OH, NO₃+RH, N₂O₅ hydrolysis,

respectively, are given by:

$$\Delta^{17}\text{O}_{\text{NO}_2+\text{OH}}(\text{NO}_3^-) = 2/3\alpha \Delta^{17}\text{O}_{\text{NO}+\text{O}_3}(\text{NO}_2) \quad (17)$$

$$\Delta^{17}\text{O}_{\text{NO}_3+\text{RH}}(\text{NO}_3^-) = 1/3(2\alpha \Delta^{17}\text{O}_{\text{NO}+\text{O}_3}(\text{NO}_2) + \Delta^{17}\text{O}(\text{O}_3^*)) \quad (18)$$

$$\Delta^{17}\text{O}_{\text{N}_2\text{O}_5\text{hydro}\ell}(\text{NO}_3^-) = 1/6(4\alpha \Delta^{17}\text{O}_{\text{NO}+\text{O}_3}(\text{NO}_2) + \Delta^{17}\text{O}(\text{O}_3^*)) \quad (19)$$

These three equations can be generalized as follow: rather than computing the instantaneous isotopic signature of each nitrate source considered, under PSS conditions, let us examine their diurnally integrated isotopic signature. It is possible to compute the α value matching the DIIS values explicitly computed, using the formalism of Eqs. (17), (18) and (19):

$$\overline{\Delta^{17}\text{O}_{\text{OH}+\text{NO}_2}(\text{NO}_3^-)} = 2/3\overline{\alpha_{\text{NO}_2+\text{OH}}} \Delta^{17}\text{O}_{\text{NO}+\text{O}_3}(\text{NO}_2) \quad (20)$$

$$\overline{\Delta^{17}\text{O}_{\text{NO}_3+\text{RH}}(\text{NO}_3^-)} = 1/3(2\overline{\alpha_{\text{NO}_3+\text{RH}}} \Delta^{17}\text{O}_{\text{NO}+\text{O}_3}(\text{NO}_2) + \Delta^{17}\text{O}(\text{O}_3^*)) \quad (21)$$

$$\overline{\Delta^{17}\text{O}_{\text{N}_2\text{O}_5\text{hydro}\ell}(\text{NO}_3^-)} = 1/6(4\overline{\alpha_{\text{N}_2\text{O}_5\text{hydro}\ell}} \Delta^{17}\text{O}_{\text{NO}+\text{O}_3}(\text{NO}_2) + \Delta^{17}\text{O}(\text{O}_3^*)) \quad (22)$$

The then defined *effective* α , denoted $\overline{\alpha}$, are specific to each nitrate production pathways, and can serve to expand the formalism defined at PSS to account for the fact that PSS does not hold to quantitatively compute the isotopic signature of atmospheric nitrate sources. Such effective α values can then be implemented in a model like GEOS-Chem (Alexander et al., 2009). Indeed, in this model implementation, the isotopic signatures of nitrate production channels were computed at a daily time resolution (B. Alexander, personal communication 2011). $\overline{\alpha_{\text{NO}_2+\text{OH}}}$ is conceptually equivalent to α_{day} as defined in Alexander et al. (2009) because this pathway proceeds during the day. Likewise, Alexander et al. (2009) defined a α_{night} value which holds for N_2O_5 hydrolysis and the $\text{NO}_3 + \text{RH}$ reactions. In the cases tested, our study indicated that $\overline{\alpha_{\text{NO}_3+\text{RH}}}$ has the same value as $\overline{\alpha_{\text{N}_2\text{O}_5\text{hydro}\ell}}$, justifying the use of a single $\overline{\alpha}$ value for “nighttime” nitrate production channels. The $\overline{\alpha}$ values extracted from data in Table 9 for the $\text{OH} + \text{NO}_2$ channel are equal to 0.73 and 0.69 for the explicit calculation and Alexander et al. (2009), respectively. For the $\text{NO}_3 + \text{RH}$ channel, the $\overline{\alpha}$ values are equal to 0.93 and 0.99, respectively. The errors in terms of DIIS, as detailed above, translate in errors in terms of $\overline{\alpha}$.

In practice, the issue associated with the computation of $\overline{\alpha_{\text{NO}_2+\text{OH}}}$ in GEOS-Chem can easily be solved as follows: rather than computing α values over an arbitrary time window which causes a systematic underestimation at least on the order of 0.04 in terms of $\overline{\alpha}$, we recommend to extend the temporal range of integration to the full length of the day (i.e., from 00:00 to 24:00 solar time), and scale the instantaneous PSS α values with the rate of reaction $\text{OH} + \text{NO}_2$. Indeed, we have shown that $\overline{\Delta^{17}\text{O}_{\text{OH}+\text{NO}_2}(\text{NO}_3^-)}$ values computed using PSS approximations match the DIIS values obtained through the explicit modeling of $\Delta^{17}\text{O}$ of NO_x and NO_y . The issue with the nighttime nitrate production channels should be solved without resorting to using photochemical steady state equations at night, since we have shown that

this leads to systematically erroneous results and is based on a scientific oxymoron. The model results show that $\Delta^{17}\text{O}_{\text{NO}_3+\text{RH}}(\text{NO}_3^-)$ and $\Delta^{17}\text{O}_{\text{N}_2\text{O}_5\text{hydro}\ell}(\text{NO}_3^-)$ do not vary significantly over night. This behavior stems from the fact that the main driver of change of $\Delta^{17}\text{O}$ of nitrate precursors, that is photochemical cycling between NO_x , HO_x and ozone is inactive at night, thereby “freezing” the $\Delta^{17}\text{O}$ signature of most reactants until dawn. Given the low sensitivity of DIIS values, and thus $\overline{\alpha}$ values, for nighttime nitrate production channels to environmental conditions such as temperature, actinic flux and NO_x levels, a conservative approach may be to use a fixed value of 0.94 for the $\overline{\alpha}$ of $\text{NO}_3 + \text{RH}$ and N_2O_5 hydrolysis, respectively. Indeed, this value corresponds to the middle of the range covered (within 0.02, minimum in summer and maximum in winter) by our model runs, spanning a wide range of atmospheric and environmental conditions.

5.2 Implication for $\Delta^{17}\text{O}(\text{H}_2\text{O}_2)$

An interesting implication of our work is the fact that under all tested environmental conditions, the model predicts non-zero $\Delta^{17}\text{O}(\text{H}_2\text{O}_2)$ even without invoking non-mass dependent fractionation through the $\text{H} + \text{O}_2$ reaction, as evidenced by Savarino and Thiemens (1999a). This significant $\Delta^{17}\text{O}(\text{H}_2\text{O}_2)$, on the order of 1‰, stems from the $\text{OH} + \text{O}_3$ reaction and could be used in the future to probe the level of photochemical activity of a given air parcel through measurements of $\Delta^{17}\text{O}(\text{H}_2\text{O}_2)$ either in the gas-phase or in rainwater, as suggested by Savarino and Thiemens (1999b).

5.3 Open questions

Two untested assumptions of this work are the hypothesis that $\Delta^{17}\text{O}(\text{O}_3)$ remains constant throughout the day, and that the thermal decomposition and photolysis of HNO_4 does not lead to any isotopic scrambling between the two molecules making up these dimers. The assumption related to the diurnal variations of $\Delta^{17}\text{O}(\text{O}_3)$ can now be addressed using field measurements carried out using a chemical probing method based upon the $\text{NO}_2^- + \text{O}_3$ reaction (Michalski and Bhattacharya, 2009; Vicars et al., 2011). As indicated above, should $\Delta^{17}\text{O}(\text{O}_3)$ exhibit significant diurnal variations, several quantitative results provided above for illustration purposes would become obsolete – note that the same would apply to all model studies carried out so far, which all assume diurnally invariant $\Delta^{17}\text{O}(\text{O}_3)$ (e.g. Michalski et al., 2003; Morin et al., 2008; Kunasek et al., 2008; Dominguez et al., 2009; Michalski and Xu, 2010; Alexander et al., 2009). Nevertheless, the methodology presented here would remain valid and the developed framework is already suited to account for diurnal variations in $\Delta^{17}\text{O}(\text{O}_3)$ (Vicars et al., 2011). The question related to the chemical mechanism operating during thermal decomposition requires advanced chemical physics modeling at the molecular scale.

Alternatively, studies on $\Delta^{17}\text{O}(\text{H}_2\text{O}_2)$ may partly solve this issue, since we have shown that $\Delta^{17}\text{O}_{\text{HO}_2+\text{HO}_2}(\text{H}_2\text{O}_2)$ is most sensitive to this assumption.

Additional sources of uncertainties have not been addressed in detail in this study, such as the impact of non-zero $\Delta^{17}\text{O}(\text{O}_2)$ and $\Delta^{17}\text{O}(\text{H}_2\text{O})$ on $\Delta^{17}\text{O}$ of reactive and secondary species: although measurable (Barkan and Luz, 2003, 2005), the $\Delta^{17}\text{O}$ of O_2 and H_2O are expected to be small and should affect negligibly the discussion presented above. We have also chosen to not propagate experimental and theoretical uncertainties associated with the $\Delta^{17}\text{O}$ transfer rate of $\Delta^{17}\text{O}(\text{O}_3)$ along with chemical reactions mostly for clarity reasons, to rather focus on the overall methodological aspects of the explicit modeling of the $\Delta^{17}\text{O}$ transfer through a full photochemical mechanism.

6 Conclusions

This study addresses in detail the question of the impact of diurnal variations of $\Delta^{17}\text{O}$ of short-lived reactive species on secondary species such as atmospheric nitrate and H_2O_2 . Using a state of the art photochemical box model, the time evolution of $\Delta^{17}\text{O}$ of NO_x , NO_y and HO_x is computed under various sets of hypotheses pertaining to the method of computing the $\Delta^{17}\text{O}$ values, reflecting different levels of simplifying approximations. Most of the conclusions of this article are drawn from model simulations carried out under clean atmospheric conditions in mid-latitudes; their broader relevance and robustness is however assessed using model simulations carried out under cold and boreal conditions, and under a 100-fold increase in initial NO_x mixing ratio.

The primary goal of this study was to demonstrate that using a detailed box-modeling study to assess the isotopic signature of various nitrate and H_2O_2 production pathways is feasible and provides relevant information to larger-scale modeling studies. In the meantime, essential features of the coupling between chemical reactions and the $\Delta^{17}\text{O}$ of key atmospheric species were described and are most likely also valid under different environmental contexts. Taking this study as an initial step, the model could rather easily be extended to account for gas/particles interactions, which are of primary importance for the budget of NO_x , and to simulate $\Delta^{17}\text{O}$ values of secondary species such as atmospheric nitrate and H_2O_2 under atmospheric contexts as different as over continents (urban polluted, tropical etc.) and under polar conditions including more complex and realistic chemical mechanisms. We believe that the present study provides the necessary framework for carrying out this work under conditions that will make it usable by larger-scale modeling studies, or for the interpretation of short-term intensive measurement campaigns using a modeling tool analogous to CAABA/MECCA.

Supplement related to this article is available online at:
[http://www.atmos-chem-phys.net/11/3653/2011/
acp-11-3653-2011-supplement.pdf](http://www.atmos-chem-phys.net/11/3653/2011/acp-11-3653-2011-supplement.pdf).

Acknowledgements. Discussions with S. K. "Bhatta" Bhattacharya, Joseph Erbland, William Vicars and Tesfaye Berhanu (CNRS – Univ. Joseph Fourier, LGGE, Grenoble, France) were useful to address issues related to the transferrable $\Delta^{17}\text{O}$ of ozone. We thank Becky Alexander (Univ. of Washington, Seattle WA, USA), Joseph Erbland, one anonymous reviewer and the scientific editor Jan Kaiser (Univ. East Anglia, Norwich, United Kingdom) for helpful comments and suggestions. SM warmly thanks François Ravetta and Slimane Bekki (Univ. Pierre et Marie Curie – CNRS, IPSL-LATMOS, Paris, France) for introducing him to atmospheric chemistry modeling. We are pleased to acknowledge funding from INSU/LEFE.

Edited by: J. Kaiser



The publication of this article is financed by CNRS-INSU.

References

- Alexander, B., Savarino, J., Kreutz, K. J., and Thiemens, M. H.: Impact of preindustrial biomass-burning emissions on the oxidation pathways of tropospheric sulfur and nitrogen, *J. Geophys. Res.*, 109, D08303, doi:10.1029/2003JD004218, 2004.
- Alexander, B., Park, R. J., Jacob, D. J., Li, Q. B., Yantosca, R. M., Savarino, J., Lee, C. C. W., and Thiemens, M. H.: Sulfate formation in sea-salt aerosols: Constraints from oxygen isotopes, *J. Geophys. Res.*, 110 (D10307), doi:10.1029/2004JD005659, 2005.
- Alexander, B., Hastings, M. G., Allman, D. J., Dachs, J., Thornton, J. A., and Kunasek, S. A.: Quantifying atmospheric nitrate formation pathways based on a global model of the oxygen isotopic composition ($\Delta^{17}\text{O}$) of atmospheric nitrate, *Atmos. Chem. Phys.*, 9, 5043–5056, doi:10.5194/acp-9-5043-2009, 2009.
- Barkan, E. and Luz, B.: High-precision measurements of $^{17}\text{O}/^{16}\text{O}$ and $^{18}\text{O}/^{16}\text{O}$ of O_2 and O_2/Ar ratios in air, *Rapid Commun. Mass Spectrom.*, 17(24), 2809–2814, 2003.
- Barkan, E. and Luz, B.: High-precision measurements of $^{17}\text{O}/^{16}\text{O}$ and $^{18}\text{O}/^{16}\text{O}$ ratios in H_2O , *Rapid Commun. Mass Spectrom.*, 19, 3737–3742, 2005.
- Bhattacharya, S. K., Pandey, A., and Savarino, J.: Determination of intramolecular isotope distribution of ozone by oxidation reaction with silver metal, *J. Geophys. Res.*, 113, D03303, doi:10.1029/2006JD008309, 2008.
- Brenninkmeijer, C. A. M., Janssen, C., Kaiser, J., Röckmann, T., Rhee, T. S., and Assonov, S. S.: Isotope effects in the chemistry

- of atmospheric trace compounds, *Chem. Rev.*, 103(12), 5125–5162, doi:10.1021/cr020644k, 2003.
- Brown, S. S., Ryerson, T. B., Wollny, A. G., Brock, C. A., Peltier, R., Sullivan, A. P., Weber, R. J., Dubé, W. P., Trainer, M., Meagher, J. F., Fehsenfeld, F. C., and Ravishankara, A. R.: Variability in nocturnal nitrogen oxide processing and its role in regional air quality, *Science*, 311, 67–70, doi:10.1126/science.1120120, 2006.
- Dominguez, G., Wilkins, G., and Thiemens, M. H.: A photochemical model and sensitivity study of the triple-oxygen isotopic ($\Delta^{17}\text{O}$) composition of NO_y , HO_x , and H_2O_2 in a polluted boundary layer, *Atmos. Chem. Phys. Discuss.*, 9, 13355–13406, doi:10.5194/acpd-9-13355-2009, 2009.
- Dubey, M. K., Mohrschladt, R., Donahue, N. M., and Anderson, J. G.: Isotope specific kinetics of hydroxyl radical (OH) with water (H_2O): testing models of reactivity and atmospheric fractionation, *J. Phys. Chem. A*, 101, 1494–1500, 1997.
- Erbländ, J., Savarino, J., Morin, S., and Frey, M. M.: The oxygen isotope anomaly ($\Delta^{17}\text{O}$) of nitrate in the Vostok ice core: insights in possible changes in NO_x oxidation pathways over the last 150 000 years, *Geophys. Res. Abstract*, 11, EGU–2009–975, talk, 2009.
- Finlayson-Pitts, B. J. and Pitts, J. N.: Chemistry of the upper and lower atmosphere: theory, experiments and applications, Academic Press, San Diego CA, USA, 2000.
- Frey, M. M., Savarino, J., Morin, S., Erbländ, J., and Martins, J. M. F.: Photolytic imprint in the nitrate stable isotope signal in snow and atmosphere of East Antarctica and implications for reactive nitrogen cycling, *Atmos. Chem. Phys.*, 9, 8681–8696, doi:10.5194/acp-9-8681-2009, 2009.
- Gromov, S., Jöckel, P., Sander, R., and Brenninkmeijer, C. A. M.: A kinetic chemistry tagging technique and its application to modelling the stable isotopic composition of atmospheric trace gases, *Geosci. Model Dev.*, 3, 337–364, doi:10.5194/gmd-3-337-2010, 2010.
- Hoag, K. J., Still, C. J., Fung, I. Y., and Boering, K. A.: Triple oxygen isotope composition of tropospheric carbon dioxide as a tracer of terrestrial gross carbon fluxes, *Geophys. Res. Lett.*, 32, L02802, doi:10.1029/2004GL021011, 2005.
- Jacob, D. J.: Introduction to Atmospheric Chemistry, Princeton University Press, Princeton, NJ, USA, 1–295, 1999.
- Janssen, C.: Intramolecular isotope distribution in heavy ozone ($^{16}\text{O}^{18}\text{O}^{16}\text{O}$ and $^{16}\text{O}^{16}\text{O}^{18}\text{O}$), *J. Geophys. Res.*, 110, D08308, doi:10.1029/2004JD005479, 2005.
- Kaiser, J., Röckmann, T., and Brenninkmeijer, C. A. M.: Contribution of mass-dependent fractionation to the oxygen isotope anomaly of atmospheric nitrous oxide, *J. Geophys. Res.*, 109, D03305, doi:10.1029/2003JD004088, 2004.
- Kaiser, J., Hastings, M. G., Houlton, B. Z., Röckmann, T., and Sigman, D. M.: Triple oxygen isotope analysis of nitrate using the denitrifier method and thermal decomposition of N_2O , *Anal. Chem.*, 79, 599–607, doi:10.1021/ac061022s, 2007.
- Kunasek, S. A., Alexander, B., Steig, E. J., Hastings, M. G., Gleason, D. J., and Jarvis, J. C.: Measurements and modeling of $\Delta^{17}\text{O}$ of nitrate in snowpits from Summit, Greenland, *J. Geophys. Res.*, 113, D24302, doi:10.1029/2008JD010103, 2008.
- Laj, P., Klausen, J., Bilde, M., et al.: Measuring atmospheric composition change, *Atmos. Environ.*, 43, 5351–5414, doi:10.1016/j.atmosenv.2009.08.020, 2009.
- Liu, Q., Schurter, L. M., Muller, C. E., Aloisio, S., Francisco, J. S., and Margerum, D. W.: Kinetics and mechanisms of aqueous ozone reactions with bromide, sulfite, hydrogen sulfite, iodide, and nitrite ions., *Inorg. Chem.*, 40(17), 4436–4442, doi:10.1021/ic000919j, 2001.
- Lyons, J. R.: Transfer of mass-independent fractionation in ozone to other oxygen-containing radicals in the atmosphere, *Geophys. Res. Lett.*, 28, 3231–3234, 2001.
- Marcus, R. A.: Mass-independent oxygen isotope fractionation in selected systems. Mechanistic considerations, *Adv. Quant. Chem.*, 55, 5–19, doi:10.1016/S0065-3276(07)00202-X, 2008.
- McCabe, J. R., Thiemens, M. H., and Savarino, J.: A record of ozone variability in South Pole Antarctic snow: The role of nitrate oxygen isotopes, *J. Geophys. Res.*, 112, D12303, doi:10.1029/2006JD007822, 2007.
- Michalski, G. and Bhattacharya, S. K.: The role of symmetry in the mass independent isotope effect in ozone, *Proc. Natl. Acad. Sci. USA*, 106, 5493–5496, doi:10.1073/pnas.0812755106, 2009.
- Michalski, G. and Xu, F.: Isotope modeling of nitric acid formation in the atmosphere using ISO-RACM: Testing the importance of nitric oxide oxidation, heterogeneous reactions, and trace gas chemistry, *Atmos. Chem. Phys. Discuss.*, 10, 6829–6869, doi:10.5194/acpd-10-6829-2010, 2010.
- Michalski, G., Savarino, J., Böhlke, J. K., and Thiemens, M. H.: Determination of the total oxygen isotopic composition of nitrate and the calibration of a $\Delta^{17}\text{O}$ nitrate reference material, *Anal. Chem.*, 74, 4989–4993, doi:10.1021/ac0256282, 2002.
- Michalski, G., Scott, Z., Kabiling, M., and Thiemens, M. H.: First measurements and modeling of $\Delta^{17}\text{O}$ in atmospheric nitrate, *Geophys. Res. Lett.*, 30, 1870, doi:10.1029/2003GL017015, 2003.
- Monks, P., Granier, C., Fuzzi, S., et al.: Atmospheric composition change-global and regional air quality, *Atmos. Environ.*, 43, 5268–5350, doi:10.1016/j.atmosenv.2009.08.021, 2009.
- Morin, S.: Interactive comment on “Quantifying atmospheric nitrate formation pathways based on a global model of the oxygen isotopic composition ($\Delta^{17}\text{O}$) of atmospheric nitrate” by B. Alexander et al., *Atmos. Chem. Phys. Discuss.*, 9, C1154–C1170, doi:10.5194/acp-9-C1154-2009, 2009.
- Morin, S., Savarino, J., Bekki, S., Gong, S., and Bottenheim, J. W.: Signature of Arctic surface ozone depletion events in the isotope anomaly ($\Delta^{17}\text{O}$) of atmospheric nitrate, *Atmos. Chem. Phys.*, 7, 1451–1469, doi:10.5194/acp-7-1451-2007, 2007.
- Morin, S., Savarino, J., Frey, M. M., Yan, N., Bekki, S., Bottenheim, J. W., and Martins, J. M. F.: Tracing the origin and fate of NO_x in the Arctic atmosphere using stable isotopes in nitrate, *Science*, 322, 730–732, doi:10.1126/science.1161910, 2008.
- Morin, S., Savarino, J., Frey, M. M., Domine, F., Jacobi, H. W., Kaleschke, L., and Martins, J. M. F.: Comprehensive isotopic composition of atmospheric nitrate in the Atlantic Ocean boundary layer from 65°S to 79°N, *J. Geophys. Res.*, 114, D05303, doi:10.1029/2008JD010696, 2009.
- Péiro-García, J. and Nebot-Gil, I.: *Ab initio* study of the mechanism of the atmospheric reaction $\text{NO}_2 + \text{O}_3 \rightarrow \text{NO}_3 + \text{O}_2$, *J. Comput. Chem.*, 24, 1657–1663, 2003.
- Sander, R., Kerkweg, A., Jöckel, P., and Lelieveld, J.: Technical Note: The new comprehensive atmospheric chemistry module MECCA, *Atmos. Chem. Phys.*, 5, 445–450, doi:10.5194/acp-5-445-2005, 2005.

- Sander, R., Baumgaertner, A., Gromov, S., Harder, H., Jöckel, P., Kerkweg, A., Kubistin, D., Regelin, E., Riede, H., Sandu, A., Taraborrelli, D., Tost, H., and Xie, Z.-Q.: The atmospheric chemistry box model CAABA/MECCA-3.0gmdd, Geosci. Model Dev. Discuss., 4, 197–217, doi:10.5194/gmdd-4-197-2011, 2011.
- Savarino, J. and Morin, S.: Handbook of Environmental Isotope Geochemistry, chap. 44, The N, O, S isotopes of oxy-anions in ice cores and polar environments, Springer-Verlag, New York, USA, 2011.
- Savarino, J. and Thiemens, M. H.: Analytical procedure to determine both $\delta^{18}\text{O}$ and $\delta^{17}\text{O}$ of H_2O_2 in natural water and first measurements, Atmos. Environ., 33, 3683–3690, 1999a.
- Savarino, J. and Thiemens, M. H.: Mass-independent oxygen isotope (^{16}O , ^{17}O and ^{18}O) fractionation found in H_xO_x reactions, J. Phys. Chem. A, 103, 9221–9229, 1999b.
- Savarino, J., Lee, C. C. W., and Thiemens, M. H.: Laboratory oxygen isotopic study of sulfur (IV) oxidation: Origin of the mass-independent oxygen isotopic anomaly in atmospheric sulfates and sulfate mineral deposits on Earth, J. Geophys. Res., 105, 29079–29088, doi:10.1029/2000JD900456, 2000.
- Savarino, J., Kaiser, J., Morin, S., Sigman, D. M., and Thiemens, M. H.: Nitrogen and oxygen isotopic constraints on the origin of atmospheric nitrate in coastal Antarctica, Atmos. Chem. Phys., 7, 1925–1945, doi:10.5194/acp-7-1925-2007, 2007.
- Savarino, J., Bhattacharya, S. K., Morin, S., Baroni, M., and Doussin, J.-F.: The $\text{NO} + \text{O}_3$ reaction: a triple oxygen isotope perspective on the reaction dynamics and atmospheric implications for the transfer of the ozone isotope anomaly, J. Chem. Phys., 128, 194303, doi:10.1063/1.2917581, 2008.
- Thiemens, M. H.: History and applications of mass-independent isotope effects, Ann. Rev. Earth Planet. Sci., 34, 217–262, doi:10.1146/annurev.earth.34.031405.125026, 2006.
- Tsunogai, U., Komatsu, D. D., Daita, S., Kazemi, G. A., Nakagawa, F., Noguchi, I., and Zhang, J.: Tracing the fate of atmospheric nitrate deposited onto a forest ecosystem in Eastern Asia using $\Delta^{17}\text{O}$, Atmos. Chem. Phys., 10, 1809–1820, doi:10.5194/acp-10-1809-2010, 2010.
- Vicars, W. C., Bhattacharya, S. K., Erbland, J., Morin, S., and Savarino, J.: Measurement of the oxygen isotope anomaly ($\Delta^{17}\text{O}$) of tropospheric ozone using a nitrite-coated filter, Anal. Chem., submitted, 2011.
- Zahn, A., Frantz, P., Bechtel, C., Groß, J.-U., and Röckmann, T.: Modelling the budget of middle atmospheric water vapour isotopes, Atmos. Chem. Phys., 6, 2073–2090, doi:10.5194/acp-6-2073-2006, 2006.
- Zhu, R. and Lin, M. C.: The self-reaction of hydroperoxy radicals: *ab initio* characterization of dimer structures and reaction mechanisms, Phys. Chem. Comm., 4, 106–111, doi:10.1039/B107602G, 2001.